

Understanding the Structural Scaling Relations of Early-Type Galaxies

L. A. Porter^{1,2}, R. S. Somerville^{3*}, J. R. Primack^{1,2}, and P. H. Johansson⁴

¹*Department of Physics, University of California, Santa Cruz, California 95064, USA*

²*Santa Cruz Institute for Particle Physics, University of California, Santa Cruz, California 95064, USA*

³*Department of Physics and Astronomy, Rutgers University, Piscataway, New Jersey 08854, USA*

⁴*Department of Physics, University of Helsinki, Gustaf Hällströmin katu 2a, FI-00014 Helsinki, Finland*

6 June 2021

ABSTRACT

We use a large suite of hydrodynamical simulations of binary galaxy mergers to construct and calibrate a physical prescription for computing the effective radii and velocity dispersions of spheroids. We implement this prescription within a semi-analytic model embedded in merger trees extracted from the Bolshoi Λ CDM N-body simulation, accounting for spheroid growth via major and minor mergers as well as disk instabilities. We find that without disk instabilities, our model does not predict sufficient numbers of intermediate mass early-type galaxies in the local universe. Spheroids also form earlier in models with spheroid growth via disk instabilities. Our model correctly predicts the normalization, slope, and scatter of the low-redshift size-mass and Fundamental Plane relations for early type galaxies. It predicts a degree of curvature in the Faber-Jackson relation that is not seen in local observations, but this could be alleviated if higher mass spheroids have more bottom-heavy initial mass functions. The model also correctly predicts the observed strong evolution of the size-mass relation for spheroids out to higher redshifts, as well as the slower evolution in the normalization of the Faber-Jackson relation. We emphasize that these are genuine predictions of the model since it was tuned to match hydrodynamical simulations and not these observations.

Key words: galaxies: interactions – galaxies: evolution – galaxies: elliptical and lenticular, cD – galaxies: formation

1 INTRODUCTION

One of the most striking and well-known aspects of the galaxy population in the local universe is the distinction between ‘early type’, or spheroid-dominated, galaxies, and ‘late type’, or disk-dominated galaxies. Classical early-type galaxies (“giant ellipticals”) in the local universe are dominated by random motions, have compact, concentrated light profiles, and are typically red and gas poor. Late-type galaxies are rotation supported, have more extended light profiles, and tend to be gas-rich, blue, and star forming. While local galaxy populations span a continuum in all of these characteristics, some properties (most dramatically color or specific star formation rate) show a pronounced bimodality (e.g.

Baldry et al. 2004; Blanton & Moustakas 2009, and references therein).

In addition, both early- and late-type galaxies obey qualitatively similar, yet distinct, *scaling relations* between their kinematic and structural properties, and mass or luminosity. For example, elliptical galaxies obey a relation between surface brightness, size, and velocity dispersion (Djorgovski & Davis 1987; Dressler et al. 1987; Faber et al. 1987), termed the Fundamental Plane (FP). This plane is tilted from the plane one would expect from a simple application of the virial theorem, indicating that further processes, such as non-homology or a varying mass-to-light ratio, must play a role (Jørgensen et al. 1996). Projections of this relationship form the familiar Faber-Jackson relation (Faber & Jackson 1976) between luminosity (or stellar mass) and velocity dispersion, and the Kormendy relation between luminosity or stellar mass

* email: somerville@physics.rutgers.edu

and radius (Shen et al. 2003). Disk galaxies show similar scaling relations, but the size-mass relation for disks has a different slope, such that spheroid-dominated galaxies are smaller at fixed mass than their disk-dominated counterparts (Shen et al. 2003). Furthermore, there is a clear correlation between galaxy kinematic and structural properties and star formation history: more massive, higher velocity dispersion early-type galaxies have older, more metal rich stellar populations (Gallazzi et al. 2006). The bulges of spiral galaxies show similar scaling relations and correlations, hinting that the formation mechanism of at least “classical” bulges may be the same as that of elliptical galaxies (Burstein et al. 1997).

Only recently have large, multi-wavelength surveys begun to characterize the *evolution* of galaxy demographics and scaling relations over a significant span of cosmic history. These surveys have shown that the stellar mass contained in red sequence (passive) galaxies has increased significantly since $z \sim 1$, while the mass in blue (actively star forming) galaxies has stayed approximately constant (Bell et al. 2007; Faber et al. 2007). This implies that active galaxies have been *transformed* into passive galaxies. Moreover, the gap between the colors of active and passive galaxies in the local universe (the “green valley”) implies that this transformation must have been fairly rapid, giving rise to the frequently heard statement that star formation is being *quenched* in these systems. These studies have recently been extended to higher redshifts ($z \sim 2-3$), showing a continuation of this trend (Brammer et al. 2011; Muzzin et al. 2013).

In addition, extensive imaging with the Hubble Space Telescope has enabled the study of galaxy structural properties and stellar populations in the rest-frame optical out to $z \sim 2$. An unexpected population of extremely compact, yet massive, galaxies has been discovered at $z \sim 2-3$, which is extremely rare in the local Universe (Daddi et al. 2005; Trujillo et al. 2007; van Dokkum et al. 2008; Cassata et al. 2013), raising the question of the nature of the descendants of these objects. The structural scaling relations for disks and spheroids also evolve over cosmic time, and the size-mass relation for early-types evolves much more rapidly with redshift than that of their disk dominated counterparts (Trujillo et al. 2006; Buitrago et al. 2008; Williams et al. 2010). This rapid increase in size is accompanied by a smaller increase in central velocity dispersion (Cappellari et al. 2009; Cenarro & Trujillo 2009; Bezanson et al. 2011), suggesting that the cores of these galaxies are in place at high redshifts. Recent observations have begun to probe the evolutionary link between diffuse star-forming galaxies and compact quiescent galaxies at high redshift. These studies have found populations of dense galaxies with high rates of star formation (Wuyts et al. 2011; Barro et al. 2013), as well as compact post-starburst galaxies (Whitaker et al. 2012) above $z \sim 1$, suggesting that these galaxies are in the process of undergoing morphological transformations and quenching.

Several different mechanisms have been proposed to explain this transformation. Hydrodynamical simulations have shown that major mergers of gas-rich galaxies can induce massive amounts of star formation, transforming a

rotation-supported disk into a pressure-supported bulge (Mihos & Hernquist 1994a,b; Barnes & Hernquist 1996; Naab et al. 2006; Cox et al. 2008). Early type galaxies can also be formed or enlarged through a sequence of multiple gas-poor (dry) minor mergers (Naab et al. 2007; Naab et al. 2009).

A number of authors have proposed an evolutionary link between the formation of a bulge, the growth of a central supermassive black hole (SMBH), and quenching of massive galaxies (e.g. Croton et al. 2006; Bower et al. 2006; Somerville et al. 2008b; Hopkins et al. 2008). The same merger-induced torques that drive gas into galaxy centers, fueling nuclear starbursts, may also drive accretion onto a SMBH, leading to a quasar or Active Galactic Nucleus (AGN). This accretion can drive powerful outflows that may clear out much of the cold gas from the remnant, quenching further star formation (Springel et al. 2005; Di Matteo et al. 2005). Once a massive SMBH is present, even small amounts of accretion may be able to produce radio jets that efficiently heat the surrounding hot gas halo, preventing future cooling and star formation (Fabian 2012, and references therein). It is interesting and suggestive, though far from conclusive, that the galaxy merger rate estimated from observations of close pairs and morphologically disturbed galaxies appears to be consistent with what would be needed to account for the growth of the quenched population, and the triggering of observed bright AGN (Hopkins et al. 2008; Robaina et al. 2010; Bundy et al. 2008).

It has been suggested that bulges may also form and grow in-situ due to internal gravitational instabilities. This process can take the form of the formation of a bar that destabilizes the disk, transferring mass into a compact, dynamically hot component (Toomre 1964; Hohl 1971; Ostriker & Peebles 1973; Combes et al. 1990). Clumps of gas may also form in the disk, and migrate inwards (Elmegreen et al. 2008; Dekel et al. 2009a; Bournaud et al. 2011) to form a bulge. However, the efficiency of bulge formation via this in-situ channel, the detailed physics of the process, and its importance relative to mergers in a cosmological context, remain poorly understood.

A general picture has emerged in which the progenitors of early type galaxies form at high redshift in one or more gas-rich “wet” mergers, and subsequently grow through predominantly dry mergers, which can build up a more diffuse bulge, while leaving the center relatively dense (e.g., Naab et al. 2007; Naab et al. 2009; Hopkins et al. 2009; Oser et al. 2010; Johansson et al. 2012). Such a picture would be consistent with observations suggesting that elliptical galaxies formed their centers rapidly, while the outer regions were accreted over longer timescales (van Dokkum et al. 2010; Forbes et al. 2011). However, this picture has not been tested quantitatively by confronting the predictions of large volume cosmological simulations with observations of galaxy demographics and scaling relations and their evolution over cosmic time.

In order to make detailed predictions regarding the connection between star formation history and internal structure for galaxy populations, it is necessary to simultaneously treat the cosmological framework of the growth

of structure through mergers and accretion, while simultaneously resolving the internal structure and kinematics of galaxies. One needs to know what kind of objects are merging, and their gas content, morphology, structure, size, accretion rate, star formation rate, etc. The dynamic range needed to simultaneously resolve galaxy internal structure while simulating cosmological volumes is currently difficult or impossible to achieve with purely numerical hydrodynamic techniques.

Traditional semi-analytic models (SAMs) make predictions for the global properties of galaxies as they form and evolve within the framework of the Λ CDM paradigm for structure formation. (Kauffmann & White 1993; Cole et al. 1994; Somerville & Primack 1999; Cole et al. 2000; Hatton et al. 2003; Croton et al. 2006; De Lucia et al. 2006; Bower et al. 2006; Somerville et al. 2008b; Fontanot et al. 2009; Benson & Bower 2010; Cook et al. 2010; Guo et al. 2011; Somerville et al. 2012). SAMs have been shown to be a useful tool for examining the evolution of galaxy morphological demographics and different channels for bulge formation in a cosmological context. For example, De Lucia et al. (2006) and Benson & Devereux (2010) have studied the build-up of the spheroid-dominated population over cosmic time. Parry et al. (2009), De Lucia et al. (2011) and Fontanot et al. (2012) have used SAMs to explore the relative importance of mergers and disk instabilities in building the population of early-type galaxies.

However, most SAMs do not provide detailed predictions about the internal structure of galaxies. A simple approach to predict the radial sizes of disk-dominated galaxies, using angular momentum conservation arguments (Mo et al. 1998), has been shown to be surprisingly successful at reproducing the evolution of the size-mass relationship for disk-dominated galaxies (Somerville et al. 2008a). But many previous attempts to model the radii and velocity dispersions of early-type galaxies have been less successful. Cole et al. (2000) applied a simple formula to predict the radii of spheroidal remnants following a major merger using the virial theorem and conservation of energy, assuming that the merging galaxies have a similar structure to the resulting spheroidal galaxy. While this relation may be correct for dissipationless gas-poor mergers, the energy lost due to star formation in gas-rich mergers results in a deviation from the virial relation, and smaller remnant radii (Cox et al. 2006; Dekel & Cox 2006; Robertson et al. 2006b).

Incorporating this dissipation is probably essential: a study using the Bower et al. (2006) SAM framework found that they were able to match the observed $z \sim 0$ spheroid size-mass relation only by including dissipation (Shankar et al. 2010; Shankar et al. 2010). Khochfar & Silk (2006) have also presented a semi-analytic model for the sizes of spheroids in which the gas fraction of the progenitors played a key role in explaining the observed size evolution and the scatter in the size-mass relation at the present day. Another recent study based on SAMs that did not include dissipation in modeling merger remnants produced a size-mass relation with too shallow a slope and too large a scatter (Guo et al. 2011).

A large body of literature has studied the structural properties of binary merger remnants in N-body plus smoothed particle hydrodynamics (SPH) simulations (Cox et al. 2006; Dekel & Cox 2006; Robertson et al. 2006b; Hopkins & Beacom 2008). While these studies have provided encouraging results regarding the explanation of spheroid scaling relations, these simulations have a number of significant limitations. They are not in a proper cosmological context and do not include a hot gas halo or cosmological accretion of gas or dark matter. The initial conditions are idealized and arbitrary, and represent only single, binary mergers, predominantly major mergers of fairly gas-rich disk-dominated progenitors. In contrast, cosmological simulations predict that multiple mergers, mixed-morphology mergers, gas-poor (“dry”) and minor mergers are all statistically important in forming the observed present day population of early-type galaxies (Moster et al. 2014; Khochfar & Burkert 2003).

Using a large suite of these binary SPH merger simulations (Cox 2004; Cox et al. 2006, 2008), Covington et al. (2008, hereafter C08) developed an analytic model to predict the effective radius and velocity dispersion following the major merger of two disk galaxies. This model was based upon the virial theorem with the incorporation of energy losses due to dissipation. In further work, Covington et al. (2011, hereafter C11) simplified the model and applied it via post-processing to mergers of disk-dominated galaxies with properties taken from the Croton et al. (2006) Millennium SAM and the Somerville et al. (2008b) SAM.

C11 showed that the C08 model reproduces the steeper slope of the size-mass relation of spheroid-dominated galaxies relative to disks, as observed. In addition the model predicts a much smaller dispersion in the size-mass relation for early-type galaxies relative to the dispersion in the corresponding relationship for the progenitor disk galaxies. This occurs because the disk galaxies with larger radius for their mass tend to be more diffuse and gas-rich, and a higher progenitor gas content leads to more dissipation during the merger, resulting in more compact remnants. In contrast, disk galaxies with smaller radii tend to be gas poor, resulting in less dissipation and less compact stellar spheroids. These effects conspire to produce remnants that are of similar sizes, irrespective of the sizes of the progenitor galaxies. In addition, the C08 model qualitatively reproduced the evolution of the size-mass relation with redshift (Trujillo et al. 2006), and correctly reproduced a tilt in the FP away from the simple virial relation. Using the methods of C08 and C11, as well as an alternative prescription in a similar spirit from Hopkins et al. (2009c), Shankar et al. (2013) reached similar conclusions.

In this paper, we develop a more complete model for predicting the size and velocity dispersion of spheroids by augmenting the initial suite of SPH merger simulations used by Covington and collaborators, which were solely for fairly gas-rich, disk-dominated progenitors, to include mergers involving spheroid-dominated and gas-poor progenitors using the simulation suite presented in Johansson et al. (2009). We present an extended version of the C08 model that accounts for these additional variables, and implement the new model self-consistently

within a full semi-analytic model. In addition, we implement a model for the sizes and velocity dispersions of spheroids formed in disk instabilities.

We make use of the ‘‘Santa Cruz’’ SAM, first presented in Somerville & Primack (1999) and significantly updated in Somerville et al. (2008b, S08) and Somerville et al. (2012, S12), now run within merger trees extracted from the Bolshoi cosmological N-body simulation (Klypin et al. 2011; Trujillo-Gomez et al. 2011) using the ROCKSTAR algorithm developed by Behroozi et al. (2013). The Santa Cruz SAM has been shown to be quite successful in predicting many properties of nearby galaxies, including the stellar mass and luminosity function (Somerville et al. 2008b, 2012), disk gas fractions, the relative fraction of disk vs. spheroid-dominated galaxies (Hopkins et al. 2009b), and the fraction of active vs. passive central galaxies as a function of stellar mass (Kimm et al. 2009). In addition, the model reproduces the evolution of the size-mass relationship for disk-dominated galaxies to $z \sim 2$ (Somerville et al. 2008a), and is consistent with observational constraints on the galaxy merger rate (Lotz et al. 2011). Hirschmann et al. (2012) showed that a version of the S08/S12 SAM with minor modifications also reproduced the evolution of the luminosity function of radiatively efficient AGN from $z \sim 5-0$. Lu et al. (2013) recently presented a comparison of three SAM codes, including the same models used here, run within the same Bolshoi-based merger trees, and showed broad agreement between the predictions of the three models. Therefore this SAM should provide a reasonably robust and reliable framework within which to predict the evolution of the properties of spheroids within a cosmological context.

The paper is arranged as follows. In Section 2 we provide a brief overview of all the physical processes in the SAM, paying particular attention to the areas where the current SAM differs from recently-published versions (Somerville et al. 2008b, 2012; Hirschmann et al. 2012). In Section 3 we present our new analysis of hydrodynamical binary merger simulations spanning a broader range of merger configurations and the extended model that we use to predict the effective radii and velocity dispersions of spheroids. As there is still considerable uncertainty in the importance of disk instabilities in producing spheroids, and the details of how this process works, we present three models: one without disk instabilities, one in which only the stellar disk participates in the instability, and one in which both gas and stars in the disk participate in the instability. In Section 4 we present the stellar mass function, bulge-to-total ratio, size-mass, Faber-Jackson, and Fundamental Plane relations for the simulated galaxies, from redshift zero to ~ 2 , and compare with available observations. We discuss the implications of our results and conclude in Section 5.

2 METHODS

Our baseline SAM is an extension of the model of Somerville & Primack (1999) and Somerville et al. (2001, 2008b, 2012). Galaxies form, evolve, and merge in a hierarchical manner, following the growth of their underlying

dark matter halos. We include prescriptions for the radiative cooling of gas, star formation, supernova feedback, black hole growth and AGN feedback, and chemical enrichment of the stars, interstellar medium (ISM), and intergalactic medium (IGM). We provide a brief summary of the recipes used here, emphasizing any relevant differences between this model and previous versions. For the full details of the SAM, we refer readers to Somerville et al. (2008b) and Somerville et al. (2012).

In this work, we make use of merger trees extracted from the Bolshoi N-Body dark matter simulation (Klypin et al. 2011; Trujillo-Gomez et al. 2011) using the ROCKSTAR method developed by Behroozi et al. (2013). The simulation is complete down to halos with virial velocity $V_{\text{circ}} = 50$ km/s, with a force resolution of $1 h^{-1}$ kpc and a mass resolution of $1.9 \times 10^8 M_{\odot}$ per particle. Most previously published versions of the Santa Cruz SAM were based on merger trees constructed using the Extended Press-Schechter (EPS) method; merger trees extracted from N-body simulations are presumably more accurate. However, we find that running the SAM with the same parameters on the EPS and Bolshoi based merger trees yields very similar results.

All results presented here assume a Λ CDM cosmology, with cosmological parameters chosen to match those adopted in the Bolshoi simulation: $\Omega_m = 0.27$, $\Omega_{\Lambda} = 0.73$, $h = 0.70$, power spectrum normalization $\sigma_8 = 0.82$, tilt $n = 0.95$ (Klypin et al. 2011). These parameter values are consistent with the Wilkinson Microwave Anisotropy Probe (WMAP) 5/7-year results (Komatsu et al. 2009, 2011).

When two dark matter halos merge we define the ‘central’ galaxy as the most massive galaxy of the larger halo, with all other galaxies termed ‘satellites.’ The satellite galaxies then lose angular momentum due to dynamical friction and merge with the central galaxy on a timescale that we estimate based on fitting functions based on numerical simulations and provided by Boylan-Kolchin et al. (2008). Satellites are tidally stripped during this process, so that satellites with long merger timescales may become tidally disrupted and destroyed before they merge with the central galaxy. In this case, the stars from the satellite are added to a diffuse stellar halo. We do not allow satellite galaxies to merge with other satellites.

2.1 Gas cooling

Gas cools and condenses from a reservoir of hot gas in the dark matter halo. Before reionization, the amount of hot gas in the halo is equal to the baryon fraction multiplied by the halo mass; once reionization begins, the amount of collapsed gas is a function of the timescale of reionization and the halo mass. We treat this quantity using a parameterization from numerical hydrodynamic simulations (Gnedin 2000; Kravtsov et al. 2004), using $z_{\text{overlap}} = 12$ as the redshift at which H II regions first overlap and $z_{\text{reion}} = 11$ as the redshift at which the universe is fully reionized.

Our cooling model is similar to the model originally proposed by White & Frenk (1991). When a halo first

collapses, the hot gas is initialized at the virial temperature of the halo and follows an isothermal density profile, $\rho_{\text{hot}}(r) = m_{\text{hot}}/(4\pi r^2 r_{\text{vir}})$, where m_{hot} is the mass of hot gas and r_{vir} is the virial radius of the halo. This gas then cools from the center to progressively larger radii on a timescale t_{cool} dependent on the density of the hot gas. We can thus define a cooling radius r_{cool} as the radius within which all the enclosed gas has had enough time to cool. This radius is calculated using the temperature- and metallicity-dependent atomic cooling curves of Sutherland & Dopita (1993).

By setting the cooling time to be equivalent to the dynamical time of the halo, we find that $t_{\text{cool}} \propto r_{\text{vir}}/V_{\text{vir}}$, where V_{vir} is the virial velocity of the halo. If the cooling radius is less than the virial radius, then solving for the mass within the cooling radius and differentiating yields a cooling rate of

$$\dot{m}_{\text{cool}} = 0.5m_{\text{hot}} \frac{r_{\text{cool}}}{r_{\text{vir}}} \frac{1}{t_{\text{cool}}}. \quad (1)$$

If the cooling rate is larger than the virial radius then the cooling rate is given by the rate at which gas is accreted into the halo,

$$\dot{m}_{\text{cool}} = 0.5m_{\text{hot}} \frac{1}{t_{\text{cool}}}, \quad (2)$$

where the factor of 0.5 is included for continuity. These two modes of gas accretion are sometimes termed ‘hot’ and ‘cold’ mode accretion, respectively. In the ‘hot’ mode gas is assumed to be shock-heated to the virial temperature of the halo, resulting in relatively long cooling times. In the ‘cold’ mode the gas is thought to penetrate the halo via filamentary streams or ‘cold flows’ (Birnboim & Dekel 2003; Kereš et al. 2005; Dekel et al. 2009a), and is never shock-heated. The transition between these two regimes is dependent on halo mass and redshift, with cold flows becoming more dominant at higher redshifts and lower halo masses.

In the SAM we associate cold gas with the central halo, so that only the central galaxy may accrete gas. Accreted satellite galaxies retain their cold gas upon their accretion into a larger halo, but this gas is typically consumed on a short timescale. This produces a population of satellite galaxies that is unrealistically red and old, as in reality, satellite galaxies may preserve some of their hot gas haloes, producing a supply of cold gas even after they are accreted. However, models that have included longer timescale accretion onto satellite galaxies have not reported large differences in the properties of central galaxies or global populations (e.g. Font et al. 2008; Guo et al. 2011), so for the massive galaxies that we focus on here, this probably will not have a major impact on our results.

2.2 Disk formation

As gas cools, we assume that it settles into a rotationally-supported exponential disk. Assuming the halo follows an NFW profile (Navarro et al. 1997) and responds adiabatically to disk formation, we can use conservation of angular momentum to find the scale radius of the disk given the halo’s concentration and spin, and the ratio of baryons in the disk to the mass of the halo. We use a

prescription based on the work of Mo et al. (1998) and described in further detail in Somerville et al. (2008a), which has been shown to reproduce the scaling relations for disk galaxies out to $z \sim 2$. However, in contrast to Somerville et al. (2008a), here we use the baryon fraction of the disk as predicted by the SAM, and assume that the predicted scale radius is the scale length of the *gas* (rather than stars) in the disk. We convert between the scale lengths of the gas and stars using $r_{\text{gas}} = \chi r_{\text{stars}}$, where $\chi = 1.7$, based on observations of nearby spiral galaxies (Leroy et al. 2008). We have verified that our new models retain good agreement with the size-mass relation for disk-dominated galaxies, and its evolution since $z \sim 2$.

2.3 Disk mode star formation

We allow for two modes of star formation: ‘disk mode’ star formation, which occurs in disks at all times as long as cold gas above a critical surface density is present, and ‘burst mode’ star formation, which occurs after two galaxies merge or (optionally) after a disk instability. Stars are assumed to form following a Chabrier (2003) initial mass function (IMF). We use an instantaneous recycling approximation to incorporate stellar mass loss; at every time-step a fraction $R = 0.43$ of the mass turned into stars is returned to the cold gas reservoir. This parameter has been shown to be a good approximation to the mass loss from massive stars in a Chabrier IMF (Bruzual & Charlot 2003).

In the ‘disk mode’ the star formation rate density is dependent on the surface density of cold gas in the disk, following the empirical Schmidt-Kennicutt relation (Kennicutt 1988, 1998). Only gas that is above a critical surface density threshold $\Sigma_{\text{crit}} = 6 M_{\odot} \text{pc}^{-2}$ is allowed to form stars. All stars that form in the disk mode are added to the disk component of the galaxy.

2.4 Mergers

‘Wet’ mergers are assumed to trigger a burst of star formation, with an efficiency that is dependent on the gas fraction of the central galaxy’s disk and the mass ratio of the two progenitors. This efficiency is parameterized based on the results of hydrodynamical simulations (Robertson et al. 2006b; Cox et al. 2008; Hopkins et al. 2009a); a higher efficiency produces a higher star formation rate and destroys a higher fraction of the disk, transferring that stellar mass to a spheroid. Following Hopkins et al. (2009a,d) the burst efficiency decreases with both mass ratio and gas fraction; in extremely gas-rich disks there is not enough stellar mass to create a torque between the gas and stars, and so the gas cannot efficiently lose its angular momentum and collapse. This is the same approximation as used in Somerville et al. (2012) but represents an improvement relative to earlier works (Somerville et al. 2008a), in which the merger efficiency was strictly a function of mass ratio.

All the stars formed in the ‘burst’ mode are added to the spheroidal component of the remnant. We also allow for a fraction $f_{\text{scatter}} = 0.2$ of the stars in the

satellite galaxy to be scattered into the diffuse stellar halo; all of the other stars in the satellite galaxy are added to the bulge. In addition, we allow a portion of the central galaxy’s stellar disk at final coalescence to be heated and become dispersion-supported. Again following Hopkins et al. (2009a,d) we set the fraction of the disk that is transferred to the spheroidal component to be equivalent to the mass ratio of the merger, which is roughly equivalent to the fraction of the central galaxy’s stellar disk that lies within the radius of the satellite galaxy at coalescence.

We note that, in addition to mergers, environmental processes such as tidal harassment (Moore et al. 1996, 1998; Gnedin 2003) and ram pressure stripping of cold gas (Gunn & Gott 1972) have been shown to drive disks towards earlier morphological types. We do not include any of these processes in our current model. However these processes are primarily expected to be significant in galaxy groups and clusters and should be sub-dominant in field galaxy samples, on which we focus here.

2.5 Supernova feedback and chemical enrichment

Massive stars and supernovae are assumed to produce winds that drive cold gas back into the ICM and IGM, heating the gas in the process. The mass outflow rate is proportional to the star formation rate,

$$\dot{m}_{\text{rh}} = \epsilon_{\text{SN}} \left(\frac{200 \text{ km s}^{-1}}{V_{\text{disk}}} \right)^{\alpha_{rh}} \dot{m}_*, \quad (3)$$

where $\epsilon_{\text{SN}} = 1.5$ and $\alpha_{rh} = 2.2$ are free parameters tuned to reproduce the slope of the stellar mass function at low masses and V_{disk} is the circular velocity of the disk, assumed to be the maximum rotation velocity of the dark matter halo (with this assumption, our disks lie on the observed Tully-Fisher relation). The proportion of the gas that is ejected from the halo entirely is a decreasing function of the halo’s virial velocity. This gas can then fall back into the hot halo, at a re-infall rate that is proportional to the mass of the ejected gas and inversely proportional to the dynamical time of the halo (see S08 for details).

We model chemical enrichment using the instantaneous recycling approximation. Whenever a mass dm_* of stars is formed, we add a mass of metals $dM_Z = y dm_*$ to the cold gas, where the chemical yield value $y = 1.5Z_{\odot}$ is a free parameter that is chosen to match the normalization of the observed mass-metallicity relation. Newly-formed stars are assumed to have the same metallicity as the mean metallicity Z_{cold} of the cold gas in the ISM at that timestep. When gas is ejected due to supernova feedback, these winds are assumed to have a metallicity Z_{cold} . Ejected metals are assumed to “re-infall” back into the hot halo on the same timescale as the gas.

2.6 Disk instabilities

It is well known that a massive dark matter halo can stabilize a fragile cold, thin disk (Ostriker & Peebles 1973; Fall & Efstathiou 1980). Early dissipationless N-body

simulations of isolated disk galaxies (Efstathiou et al. 1982) showed that if the mass of stars in the disk exceeded a critical value relative to the mass of dark matter, the disk could become unstable and form a bar. Bars can buckle and form bulges (Debattista et al. 2004).

Several previous SAMs have adopted a “disk instability” mode for bulge formation and growth, based on a Toomre-like (Toomre 1964) condition to determine the onset of instability as suggested by Efstathiou et al. (1982). We define

$$\epsilon_{\text{disk}} = \frac{V_{\text{max}}}{(GM_{\text{disk}}/r_{\text{disk}})^{1/2}}, \quad (4)$$

where V_{max} is the maximum circular velocity of the halo, r_{disk} is the scale length of the disk, and M_{disk} is the mass of the disk (note we discuss more precise definitions of these quantities in a moment). Then in any timestep in which $\epsilon_{\text{disk}} < \epsilon_{\text{crit}}$, the disk is declared to be ‘unstable’. Numerical simulations of idealized, isolated disks suggest that the value of ϵ_{crit} is in the range of 0.6-1.1, with disks containing cold gas having a lower instability threshold than pure stellar disks (Efstathiou et al. 1982; Christodoulou et al. 1995; Mo et al. 1998; Syer et al. 1999).

Different modelers diverge rather dramatically in deciding the details of how this criterion is implemented and what the consequences of a declaration of instability should be. Some modelers use the stellar mass of the disk as M_{disk} in the formula above, while others use the sum of the stars and cold gas in the disk. When the disk is declared to be unstable, some (e.g. Guo et al. 2011) move just enough stars from the disk component to the spheroid component to achieve marginal stability; others (e.g. Bower et al. 2006) move *all* of the stars and cold gas in the disk to a bulge component. Unsurprisingly, these workers differ significantly in their conclusions regarding the importance of disk instabilities for bulge growth. Moreover, Athanassoula (2008) has argued that this criterion is in any case insufficient to determine the onset of bar formation.

In addition to this “classical”, bar-driven mode of in-situ bulge growth, cosmological hydrodynamical simulations (e.g. Dekel et al. 2009b; Ceverino et al. 2010) have shown that gas-rich disks can undergo dramatic fragmentation due to “violent disk instabilities” (VDI). In VDI, gravitational instabilities lead to the formation of giant clumps in the disk, which appear qualitatively similar to the structures that are frequently observed in high redshift disks (Elmegreen et al. 2009; Genzel et al. 2011; Guo et al. 2012; Wuyts et al. 2012). These clumps may then migrate to the center of the galaxy, providing an alternative pathway for bulge growth (Elmegreen et al. 2008; Dekel et al. 2009b; Bournaud et al. 2011). Disks are more susceptible to VDI at high redshift, where the accretion rate and gas fractions are high (Dekel et al. 2009b). While there has been recent progress in studying this process, the amount of mass actually transferred to the bulge is highly sensitive to the effectiveness of stellar-driven winds. In simulations with strong stellar feedback, many of the clumps tend to be destroyed before they reach the center of the galaxy (Genel et al. 2012b), so they probably contribute little to the bulge. However,

the implementation of these feedback processes in galaxy-scale simulations remains highly uncertain.

Keeping in mind these large uncertainties, we consider three ways of treating disk instabilities in this paper. In the first (**‘No DI’**), we neglect disk instabilities and allow bulges to form and grow only through mergers. This case corresponds to most previously published versions of the Santa Cruz SAM (e.g., S08, S12). In our second model variant (**‘Stars DI’**), we use the radius and mass of the stellar disk as r_{disk} and M_{disk} in Eqn. 4 above, and in each timestep in which the disk is deemed to be unstable, we move *stars only* from the disk to the spheroid component until $\epsilon_{\text{disk}} = \epsilon_{\text{crit}}$. In our third model variant (**‘Stars+Gas DI’**), we use the radius of the *gas disk* and the *mass of stars and cold gas* in the disk as r_{disk} and M_{disk} in Eqn. 4 above. In each timestep in which the disk is deemed to be unstable, we move *stars and gas* from the disk to the spheroid component to achieve marginal stability, and the cold gas that is moved to the spheroid is assumed to participate in a starburst. If we define the total mass of gas and stars that is moved from the disk to the bulge to be Δm_{bulge} , then the mass of cold gas that is moved to the bulge is $\Delta m_{\text{bulge,gas}} = f_{\text{cold,disk}} \Delta m_{\text{bulge}}$, where $f_{\text{cold,disk}} \equiv m_{\text{cold,disk}} / (m_{\text{cold,disk}} + m_{\text{star,disk}})$ is the cold gas fraction in the disk. The efficiency and timescale of the starburst is computed using the same approach as for merger-triggered bursts. In both models, we use the maximum circular velocity of the (unmodified) dark matter halo as V_{max} in Eqn. 4.

Our implementation of the ‘Stars DI’ model is very similar to that used by other authors such as De Lucia et al. (2011) and Guo et al. (2011). Our ‘Stars+Gas DI’ model is intended to schematically represent a VDI-like situation, which is driven largely by the inflow of cold gas. In practice, because we restore the disk to marginal stability in each timestep in which it is determined to be unstable, especially at high redshift the disk tends to become unstable again in the next timestep due to accretion of new gas which grows the disk above the critical mass again, producing a cascade of instability events in the SAM.

In agreement with some previous studies, we find that our ‘No DI’ model does not appear to produce enough intermediate mass early-type galaxies at $z = 0$, and that this agreement is improved by switching on the disk instability mode for bulge growth (Guo et al. 2011; De Lucia et al. 2011; Shankar et al. 2013). We therefore tune our model by adjusting ϵ_{crit} to reproduce the observed stellar mass function of early-type galaxies in the local universe. We adopted $\epsilon_{\text{crit}} = 0.75$ in the ‘Stars DI’ model and 0.70 in the ‘Stars+Gas DI’ model, which is within the expected range of values suggested by the simulations discussed above.

2.7 Black Hole Accretion

Each galaxy is seeded with a ‘heavy’ black hole (Loeb & Rasio 1994; Koushiappas et al. 2004; Volonteri & Stark 2011), with a mass $10^5 M_{\odot}$. In all of our models, as in S08, rapid black hole accretion leading to radiatively efficient AGN activity is triggered

by mergers. When two galaxies merge, their black holes are assumed to merge as well. As the two galaxies approach coalescence the black hole begins to accrete and radiate, depositing energy into the ISM. The black hole accretes at the Eddington rate until it exceeds a critical mass; this mass corresponds to the energy needed to halt further accretion and begin to power a pressure-driven outflow. The accretion rate then declines as a power law, following the lightcurves derived from numerical simulations by Hopkins et al. (2006). For more details, see Hirschmann et al. (2012).

Following Hopkins et al. (2007), the critical mass is given by

$$\log \left(\frac{M_{\text{crit}}}{M_{*,\text{bulge}}} \right) = f_{\text{BH,crit}} [-3.27 + 0.36 \operatorname{erf}((f_{\text{gas}} - 0.4)/0.28)], \quad (5)$$

where $M_{*,\text{bulge}}$ is the stellar mass of the bulge, f_{gas} is the cold gas fraction of the larger merger progenitor, and $f_{\text{BH,crit}}$ is a tunable parameter of order unity, set to reproduce the redshift zero relationship between the mass of the black hole and the mass of the stellar bulge (McConnell & Ma 2013). This fitting function is based on an analysis of a large suite of SPH simulations of binary mergers including BH growth and AGN feedback, as described in Hopkins et al. (2007). If the sum of the two pre-existing black holes is already larger than the critical mass, then the BH goes immediately into the ‘blowout’ phase (i.e., the accretion rate starts at Eddington but immediately begins to decline). Note that this is slightly different from the implementation in S08 and Hirschmann et al. (2012), in which if the initial BH mass was larger than the critical mass, no accretion onto the BH was triggered at all. The new treatment is a more realistic representation of what actually happens in the hydrodynamic simulations (P. Hopkins, priv. comm.).

In the ‘Stars DI’ and ‘Stars+Gas DI’ models, black holes are also allowed to grow following a disk instability. As with mergers, the growth of the black hole is limited by the amount of low angular momentum material in the center of the galaxy following an instability event. We limit this term to be a fraction $f_{\text{fuel,DI}} = 0.002$ of the mass that is transferred from the disk to the bulge. Following a DI event, the BH accretes until this fuel is consumed. However, as noted above, the high gas inflow rate at high redshifts tends to produce gas-rich disks that are unstable for extended periods of time in the ‘Stars+Gas DI’ model. Allowing the black hole to accrete at the Eddington rate whenever the disks are unstable would produce black holes that are too massive at high redshifts, and too many luminous AGN. Therefore, following Hirschmann et al. (2012), we limit the DI-triggered black hole accretion rate to be a fraction of the Eddington limit. We choose this fraction to have a mean of $f_{\text{Edd,DI}} = 0.01$, and to have a Gaussian scatter from timestep to timestep of 0.2, representing the likely stochasticity of the BH accretion. This choice reproduces the AGN luminosity function from $z \sim 6-0$ (Hirschmann et al. in prep) and also still reproduces the BH mass bulge mass relation at $z = 0$. However, bulges and also BH form earlier in the ‘Stars+Gas DI’ model, so we must also decrease $f_{\text{BH,crit}}$ to 0.6 in the merger triggered BH accretion

mode (Eqn. 5) to maintain the agreement with the observed $m_{\text{BH}} - m_{\text{bulge}}$ relation.

Black holes are also allowed to grow via Bondi-Hoyle accretion (Bondi 1952) from the hot halo. This typically very sub-Eddington mode of accretion is associated with heating of the hot gas via giant radio jets, in what is sometimes called ‘radio mode’ feedback. The strength of the ‘radio mode’ feedback is governed by a tunable parameter κ_{radio} (see S08 for the precise definition), which we tuned independently in all three models to reproduce the knee and high-mass end of the stellar mass function.

3 MODEL FOR STRUCTURAL PARAMETERS OF SPHEROIDS

3.1 Effective radius

We first consider spheroids that are formed in mergers. In the case of a merger without dissipation, simple conservation of energy arguments would predict that the internal energy of the two progenitors is conserved during the merger:

$$E_{\text{init}} = E_f = C_{\text{int}} \sum_{i=1}^2 G \frac{(M_{*,i} + M_{\text{new},i})^2}{R_{*,i}} = C_{\text{int}} G \frac{M_{*,f}^2}{R_{*,f}}, \quad (6)$$

where $M_{*,i}$ is the stellar mass of each of the two progenitors, $M_{\text{new},i}$ is the mass of stars formed during the merger, $R_{*,i}$ are the three dimensional effective radii of the progenitors, $M_{*,f}$ and $R_{*,f}$ are the stellar mass and 3D effective radius of the merger remnant, and C_{int} is a dimensionless constant relating the internal energy of the galaxy to GM^2/R . However, in the presence of gas, mergers can be highly dissipative, inducing large amounts of star formation (Dekel & Cox 2006; Robertson et al. 2006a; Hopkins et al. 2009d); thus the conservation of energy relation must be modified with a term incorporating radiative losses. We note that the parameter C_{int} in equation 6 may actually have a degree of dependence on the morphology of the galaxy, but we have not attempted to account for that here.

Motivated by the results of hydrodynamical binary merger simulations (Cox et al. 2006, 2008), Covington et al. (2008) provided a simple parameterization of this radiative energy loss:

$$E_{\text{rad}} = C_{\text{rad}} \sum_{i=1}^2 K_i f_{g,i} f_{k,i} (1 + f_{k,i}), \quad (7)$$

where K_i , $f_{g,i}$, and $f_{k,i}$ are the total kinetic energy, baryonic gas fraction, and fractional impulse of progenitor i , C_{rad} is a dimensionless constant and the sum is over the two progenitors. Adding this term to the left hand side of equation 6 provides a natural way to incorporate dissipation in the calculation of the effective radius of elliptical galaxies ($E_{\text{init}} + E_{\text{rad}} = E_f$). Mergers with higher amounts of dissipation and star formation produce remnants with smaller effective radii, allowing for the creation of compact elliptical galaxies from diffuse spiral galaxies.

These two formulae have previously been shown to provide accurate predictions for the effective radii of elliptical galaxies resulting from the gas-rich mergers of spiral

galaxies (Covington et al. 2008, 2011). In this case, the constants C_{rad} and C_{int} were measured by fitting the relations to a suite of hydrodynamical merger simulations (Cox et al. 2006, 2008). Incorporating a simplified version of these formulae in semi-analytic models has been shown to reproduce the size-mass relation of early-type galaxies (Shankar et al. 2013; Covington et al. 2011).

The model presented in Covington et al. (2008) and Covington et al. (2011) was limited in that it was only calibrated against simulations of fairly gas-rich mergers of disk-dominated progenitors. Here, we wish to implement the model self-consistently within a full SAM, in which mergers between galaxies with a wide variety of initial gas fractions and morphologies are predicted to occur. Therefore we extend the model using an additional 68 hydrodynamical simulations of binary mergers, described in Johansson et al. (2009), and carried out using the GADGET-2 Smoothed Particle Hydrodynamics (SPH) code (Springel 2005). The simulations adopt the sub-grid ISM model of Springel & Hernquist (2003), and the Springel et al. (2005) treatment of BH growth and AGN feedback via thermal heating. A strongly pressurized ‘‘stiff’’ Effective Equation of State is adopted, to allow for construction of stable gas rich disks, following Springel (2005). Stellar driven winds are not included. These ingredients are similar to those adopted in the Cox et al. simulations used in the analysis of Covington et al., but with the addition of BH growth and AGN feedback.

This suite includes major (mass ratio $> 3:1$) and minor mergers between two disk-dominated galaxies (D-D, D-d), and between a disk-dominated and spheroid-dominated galaxy (B-D, B-d). It also contains major mergers between two spheroid-dominated galaxies (B-B); the only permutations lacking are minor mergers between two spheroid-dominated galaxies (B-b), and mergers between a larger disk-dominated galaxy and a smaller spheroid-dominated galaxy (D-b).

The spheroid-dominated progenitor galaxies were formed from mergers of disk-dominated galaxies with gas fractions ranging from 20% to 80%, producing a range of stellar masses and gas fractions in all of the mergers. We have measured the three-dimensional half-mass effective radii of these merger remnants directly, and used these values to perform a χ^2 fit to constrain C_{int} and C_{rad} . We calculate C_{int} and C_{rad} independently for the five categories of mergers described above.

Results are shown in Table 1 and Figure 1. The value of $f_{\text{rad}} \equiv C_{\text{rad}}/C_{\text{int}}$ can be thought of as characterizing the relative importance of dissipation; high values indicate more dissipation. We find that this value is highest for major mergers of two disk-dominated galaxies ($f_{\text{rad}} = 5.0$), is lower for minor mergers between two disk-dominated galaxies ($f_{\text{rad}} = 2.7$) and is zero for mergers where one or both of the galaxies is spheroid-dominated. This latter subset of mergers is thus essentially dissipationless; considering the average baryonic gas fraction in this group of mergers is 5.5% this is not an unexpected result. We note that the largest disk-disk merger remnants are much larger than predicted; these galaxies had high gas fractions before the mergers, and large amounts of star formation during the mergers. Thus these outliers

Merger	C_{int}	C_{rad}	Number
D-D	0.50	2.50	18
D-d	0.50	1.35	18
B-D	1.00	0.00	11
B-d	1.00	0.00	8
B-B	1.00	0.00	11

Table 1. Best-fit calculations of C_{int} and C_{rad} for the Johansson et al. (2009) hydrodynamical simulations. Progenitor types B and D designate bulge- and disk-dominated galaxies, respectively. Capital (lowercase) letters denote the larger (smaller) galaxy; capital-capital pairs indicate a major merger, capital-lowercase pairs indicate a minor merger. Lower values of $C_{\text{rad}}/C_{\text{int}}$ represent mergers with less dissipation; mergers where $C_{\text{rad}} = 0.0$ are essentially dissipationless.

may be an indication that the model breaks down in the most extreme merger events.

3.2 Velocity dispersion

We use the virial theorem to determine the line-of-sight velocity dispersion of the remnant:

$$\sigma^2 = \left(\frac{C_\sigma G}{2R_f} \frac{M_{*,f}}{(1 - f_{\text{dm},f})} \right), \quad (8)$$

where $M_{*,f}$ is the stellar mass of the remnant (or the single galaxy, in the case of disk instabilities), R_f is the stellar half-mass radius of the remnant, and C_σ is a dimensionless constant that accounts for the conversion between the three-dimensional effective radius and the line-of-sight projection of the velocity dispersion. We define M_{dm} to be the mass of dark matter within R_f , and $f_{\text{dm},f} = M_{\text{dm}}/(0.5M_{*,f} + M_{\text{dm}})$ to be the central dark matter fraction of the remnant (i.e. the proportion of mass within the stellar effective radius that is dark matter). Thus the term $0.5M_{*,f} + M_{\text{dm}} = 0.5M_{*,f}/(1 - f_{\text{dm},f})$ represents the total amount of stars and dark matter within the stellar half-mass radius.

We have calculated C_σ using a least-squares fit for the five categories of merger simulations described above. Stellar velocity dispersions were measured within the half-mass radius, using the average of 50 random line-of-sight projections. In this fit, the ‘true’ (rather than the ‘predicted’) half-mass radius from the simulations was used. In all cases, the value of C_σ was between 0.29 and 0.31; thus we adopt the value $C_\sigma = 0.30$ for all mergers. Results are shown in Figure 2. We find that this model quite accurately reproduces the velocity dispersions of merger remnants.

3.3 Implementation within the SAM

We apply these prescriptions in the SAM whenever two galaxies with a mass ratio greater than 1:10 merge (in mergers more minor than 1:10, the satellite material is added to the disk component as indicated by simulations). As the hydrodynamical merger suite does not contain minor mergers below a 1:6 mass ratio, we note that

the prescription for effective radius and velocity dispersion has not been tested for mergers between 1:6 and 1:10, which are actually very common. For the two merger cases not covered by our simulation suite, spheroid-spheroid minor mergers (B-b) and disk-spheroid minor mergers between a larger disk and a smaller spheroid (D-b), we adopt $C_{\text{rad}} = 0.0$, $C_{\text{int}} = 1.0$, and $C_{\text{rad}} = 1.35$, $C_{\text{int}} = 0.5$ respectively. We expect that the morphology of the secondary galaxy will not have a major effect on the remnant in minor mergers.

We assume orbital parameters for the merger following a statistical distribution (Wetzel 2010) that is dependent on the redshift of the merger and the mass of the halo containing the more massive progenitor. Whereas in the hydrodynamical simulations we were able to measure the contribution of dark matter within one effective radius directly, in the SAM we assume that the two dark matter halos merge dissipationlessly and that the remnant halo follows an isothermal profile. Strong lensing studies suggest this to be a reasonably accurate model for massive early-type galaxies (Auger et al. 2010).

The above formulae have only been calibrated against hydrodynamical simulations of binary mergers, but in the SAM we may also form a stellar bulge through disk instabilities. In this case we follow the prescription of Guo et al. (2011), assuming that the new bulge mass forms from the center of the stellar disk, which has an exponential surface density profile: $\Sigma(r) = \Sigma_0 \exp(-r/r_d)$, $\Sigma_0 = M_d/2\pi r_d^2$, where M_d is the mass of the disk and r_d is the scale length of the stellar disk. The radius r_{pb} of the disk enclosing this proto-bulge is then found by solving:

$$M_{\text{pb}} = \frac{M_d}{r_d} \left[r_d - e^{-\frac{r_{\text{pb}}}{r_d}} (r_d + r_{\text{pb}}) \right], \quad (9)$$

for r_{pb} where M_{pb} is the mass of the disk transferred to the bulge in the instability event. We then assume that this stellar proto-bulge merges dissipationlessly with any existing bulge.

Having calculated the radius of the bulge following the disk instability, we model velocity dispersion using the same extension of the virial theorem that we use for mergers.

We compute an effective radius for the composite bulge plus disk system by calculating a stellar mass- or light-averaged radius:

$$r_{\text{eff}} = (r_{\text{eff},d}M_d + r_{\text{eff},b}M_b)/(M_d + M_b) \quad (10)$$

where $r_{\text{eff},d} = 1.67 r_d$ is the effective radius of the disk, $r_{\text{eff},b}$ is the effective radius of the spheroid, and M_d and M_b are the stellar mass or luminosity of the disk and spheroid, respectively. We have found that this simple approach agrees well with more detailed modeling of the effective radius of composite spheroid plus disk systems. We use a rest-frame r -band luminosity weighting throughout this paper, but find nearly indistinguishable results when using stellar mass weighting.

We then convert our 3D radii to 2D projected radii, using the same approach as that suggested by Shankar et al. (2013). This approach relies on the tabulated form factors computed by Prugniel & Simien (1997). These factors $S(n)$ relate the gravitational en-

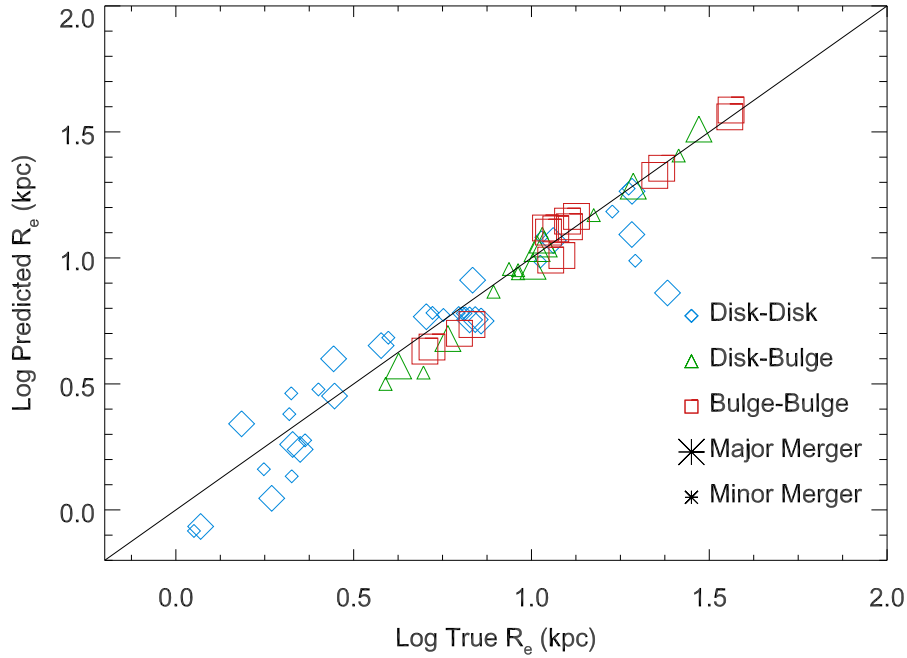


Figure 1. Predicted versus measured effective radius for the merger remnants of Johansson et al. (2009). The constants C_{int} and C_{rad} were calibrated independently for major (large symbols) and minor (small symbols) mergers, depending on the morphology of the progenitors (see Table 1). Blue diamonds represent mergers between two disk-dominated galaxies, green triangles represent mergers between a disk-dominated and a spheroid-dominated galaxy, and red squares represent mergers between two spheroid-dominated galaxies.

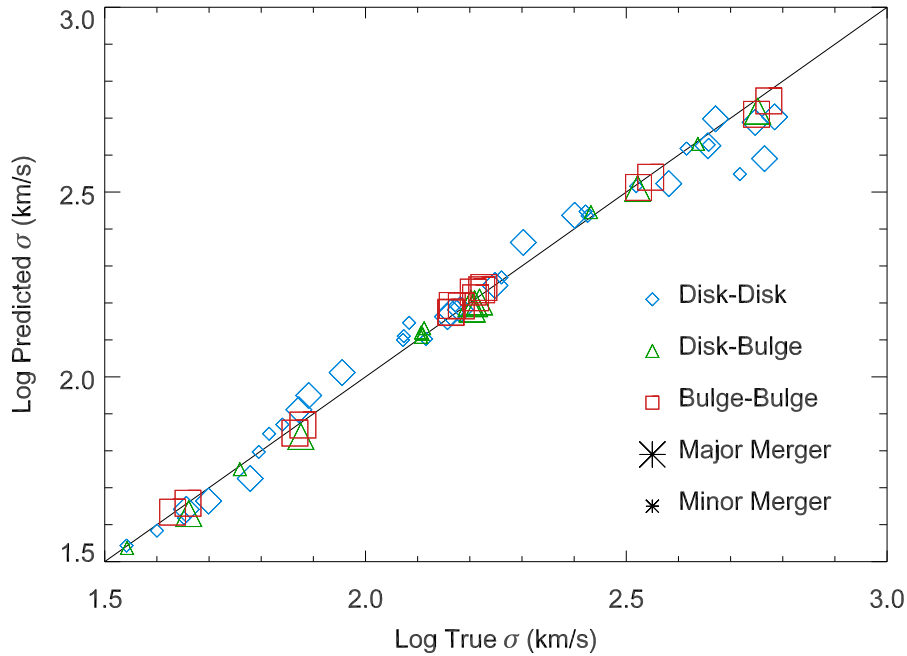


Figure 2. Predicted versus measured velocity dispersion for the merger remnants of Johansson et al. (2009). The constant C_{σ} was calibrated independently for major (large symbols) and minor (small symbols) mergers, depending on the morphology of the progenitors. All calibrations resulted in values $0.29 < C_{\sigma} < 0.31$; we adopt $C_{\sigma} = 0.30$ for all mergers. Blue diamonds represent mergers between two disk-dominated galaxies, green triangles represent mergers between a disk-dominated and a spheroid-dominated galaxy, and red squares represent mergers between two spheroid-dominated galaxies.

ergy $|W|$ to the effective radius R_e , for a system of total mass M and with Sérsic index n :

$$|W| = S(n) \frac{GM^2}{R_e} = \frac{GM^2}{R_g}, \quad (11)$$

where R_g is the gravitational radius. If the system is virialized, we can adopt the approximation $R_g \simeq 2r_{\text{eff},3\text{D}}$. The projected radius is then given by:

$$R_e = 2 S(n) r_{\text{eff},3\text{D}} \quad (12)$$

where $r_{\text{eff},3\text{D}}$ is the 3D effective radius. We adopt $S(n) = 0.34$ from Prugniel & Simien (1997), appropriate for a Sérsic index of $n = 4$. However, the dependence on Sérsic index is weak, so we adopt this conversion factor for both spheroids and disks.

An additional issue in comparing with observations is that our radii are estimated in terms of the stellar mass, while most observational studies have measured the radial extent of the *light*. Szomoru et al. (2012) found that the radius of the stellar mass distribution in galaxies of all types is on average 20-30% smaller than that of the rest-frame g -band light, with no strong apparent trends with galaxy properties or redshift, though their sample was fairly small. We do not apply this correction here, but we should keep in mind that the absolute normalization of the observational size estimates could shift by this much.

4 RESULTS

Because of the uncertainties surrounding the formation of bulges through disk instabilities discussed above, we present results for the three different treatments of this process as described in Section 2.6: ‘No DI’, ‘Stars DI’, and ‘Stars+Gas DI’. In the ‘No DI’ models, bulges can only grow through mergers, while in the ‘Stars DI’ model, stars can be moved from the disk to the bulge, and in the ‘Stars+Gas DI’ model, both stars and gas can be moved from the disk to the bulge, and gas moved to the bulge participates in a starburst. In addition, in the ‘Stars DI’ model, the DI criterion is determined only by the properties of the stellar disk, while in the ‘Stars+Gas DI’ model, the DI criterion depends on the mass of both stars and gas in the disk. We tune the above-mentioned parameters for black hole growth and disk instabilities to reproduce the stellar mass function and black hole-stellar bulge mass scaling relations at redshift zero. In the two DI models we apply the additional constraint of the fraction of spheroid-dominated galaxies as a function of stellar mass at $z = 0$, to fix the instability parameter (ϵ_{crit}), as we now describe.

4.1 Model Calibration

We first consider the stellar mass function for all galaxies (Figure 3). As discussed in Section 2.7, the efficiency of the radio mode feedback in quenching star formation is tuned independently in all three models to reproduce the knee and high-mass end of the mass function as estimated by Moustakas et al. (2013). We note that all of the models either fall slightly below the knee of the observed stellar mass function or lie slightly above the observed

high-mass turnover. This is an indication of the tension between matching the turnover and the high-mass cutoff of the mass function; increasing the strength of the radio mode feedback can provide a better match to the high-mass end but then underpredicts the knee of the stellar mass function.

However, the observational estimates of the stellar mass function at the high mass end are highly uncertain. To illustrate this, we also show the observed stellar mass function of Bernardi et al. (2013), which estimates the total light from the galaxy using a combination of a Sérsic and exponential profile. The results differ both in the estimated luminosities, due to different choices for how to do the photometry and background subtraction, and also in the assumed stellar mass-to-light ratios. We could tune our model to instead match the Bernardi et al. (2013) mass function, simply by reducing the strength of the AGN feedback, but due to the remaining uncertainties in the observations, we choose to retain the more conventional normalization for this work.

We now turn to the mass function divided by galaxy morphological type. The only morphological information provided by our SAM is the mass or luminosity of stars in the disk and spheroidal components, or equivalently a bulge-to-total ratio (B/T). It is not entirely straightforward to determine how to compare this with the most robust and widely available observational morphological classifications. These include ‘Hubble types’ based on visual classifications, concentration (usually defined as the radius containing 90 percent of the light divided by that containing 50%) or Sérsic indices based on the light profiles, and bulge-disk decompositions. Unfortunately, we were unable to locate any published stellar mass functions divided according to a B/T determined from a bulge-disk decomposition, which would be the most straightforward to compare with our predictions. We chose to use observational stellar mass functions divided by r -band concentration ($c_r \equiv r_{90}/r_{50}$). Gadotti (2009) found, based on a sample of 1000 galaxies from the Sloan Digital Sky Survey (SDSS) with bulge-disk decompositions, that B/T correlates more tightly with c_r than with Sérsic index. However, Cheng et al. (2011) found in an analysis of SDSS galaxies that concentration-selected samples can include a significant population of Sa and S0 galaxies in addition to true ellipticals. Moreover, many visually classified disks have $B/T > 0.5$. We will use B/T to define spheroid-dominated galaxies, which we refer to more or less interchangeably as ‘early types’, but we should keep in mind the difficulty of selecting the same types of objects in the observations.

It is also unclear what value of B/T we should use to define our sample of ‘early types’. Guo et al. (2011) argue that a B/T of 0.2 should correspond to a concentration of 2.86, which is a commonly used value to define ‘early type’ galaxies (e.g. Shen et al. 2003). Based on an eyeball fit to the plot of B/T versus concentration shown in Gadotti (2009), $c_r \simeq 2.6$ – 2.9 would correspond to $B/T \simeq 0.4$, though it is clear from the figure that selecting galaxies via concentration is not equivalent to a clean cut in B/T . González et al. (2009) predict based on model galaxies taken from the GALFORM semi-analytic model that galaxies with $c_r = 2.86$ may

have a broad range of values of B/T ranging from about 0.25 to about 0.65. Figure 9 of Cheng et al. (2011) shows that a galaxy sample selected with $c > 2.9$ would be expected to contain a significant population of galaxies with $0.2 < B/T < 0.5$. Many other studies adopt higher values of $B/T \sim 0.5\text{--}0.7$ to define early types (Shankar et al. 2013; Wilman et al. 2013).

Figure 4 shows the stellar mass function predicted by our three models with different recipes for bulge formation: ‘No DI’, ‘stars DI’ and ‘stars+gas DI’, compared with the observational estimate of the stellar mass function for spheroid-dominated galaxies from Bernardi et al. (2010). We compare galaxies selected with $B/T > 0.5$ with the observed mass function for $c_r = 2.86$, and we also assign concentrations to our model galaxies using a simple empirical scaling from the results of Gadotti (2009): $c_r = 2.0 + 2.4 B/T$ for $B/T < 0.5$; and $c_r = 3.0$ for $B/T > 0.5$, plus a Gaussian random deviate with $\sigma = 0.2$. We can see that these two approaches yield similar results. Moreover, we see that the model in which spheroids can only grow via mergers has too few intermediate-mass ($10^{10} < M_\odot < 10^{11}$) early-type galaxies. A similar result has been found in other SAMs (Parry et al. 2009; De Lucia et al. 2011), which use different prescriptions for spheroid growth in disk instabilities and mergers. In contrast our ‘Stars DI’ and ‘Stars+Gas DI’ models match the observed early-type mass function fairly well for galaxies with $m_* \gtrsim 10^{10} M_\odot$.

Figure 5 shows the fraction of spheroid-dominated galaxies for several other cuts in B/T or concentration, along with observational estimates. The Hyde & Bernardi (2009) sample of early type galaxies is selected via the SDSS parameter `fracDev=1` (fraction of light well-fit by a de Vaucouleur profile) and r -band axis ratio $b/a > 0.6$; we assume that this corresponds approximately to $B/T > 0.7$ for our model comparison. The Cheng et al. (2011) early-type sample is selected using an automated classification method based on image smoothness, axial ratio, and concentration and tuned to match the results of human visual classification. They state that their early-type sample corresponds approximately to $B/T > 0.5$, $c > 2.9$, so we plot it in our $c > 2.86$ panel. In all cases, the ‘No DI’ model significantly underproduces spheroid-dominated galaxies at intermediate masses, while the models with bulge formation via disk instabilities perform much better in this regard (though too many spheroid-dominated galaxies appear to be produced at low masses). Although the uncertainties are still considerable, these results are suggestive that mergers may not be the only significant channel for building spheroids. We reiterate, however, that there are still significant differences in the morphological fractions derived from observations using different classification methods, and none of the current comparisons are able to directly compare the theoretically predicted quantity (B/T) with observations, making it difficult to obtain precise and robust constraints on the models. This is clearly an area where further work is required.

However, Figure 6 shows that our current implementation of spheroid growth in disk instabilities may not be completely accurate either. This figure shows the distribution of bulge-to-total ratios measured in the H -

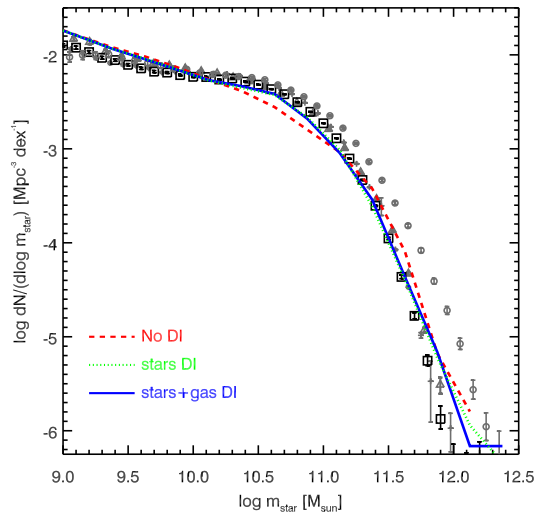


Figure 3. The galaxy stellar mass function at redshift zero. The three colored lines show the ‘No DI’ (red), ‘Stars DI’ (green) and ‘Stars+Gas DI’ (blue) models. The symbols show observational estimates of the stellar mass function of nearby galaxies (Moustakas et al. (2013): squares; Li & White (2009): triangles; Panter et al. (2007): crosses; Bernardi et al. (2013): circles).

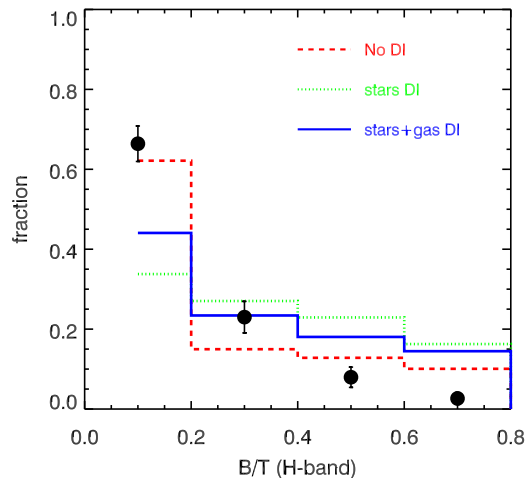


Figure 6. The distribution of rest frame H -band bulge-to-total ratios for disk-dominated galaxies ($B/T < 0.75$) with stellar masses greater than $10^{10} M_\odot$. The three colored lines show the ‘No DI’ (red), ‘Stars DI’ (green) and ‘Stars+Gas DI’ (blue) models. Symbols show the observational estimates of Weinzirl et al. (2009). Models with bulge formation via disk instabilities underpredict the fraction of disks with very small bulges ($B/T < 0.2$).

band for a sample of disk-dominated galaxies with $m_* > 10^{10} M_\odot$ by Weinzirl et al. (2009), compared with our model predictions. As Weinzirl et al. (2009) and other workers have emphasized, about 60% of even these relatively massive disks have very small bulges ($B/T < 0.2$). Our ‘No DI’ models do reproduce these results, showing

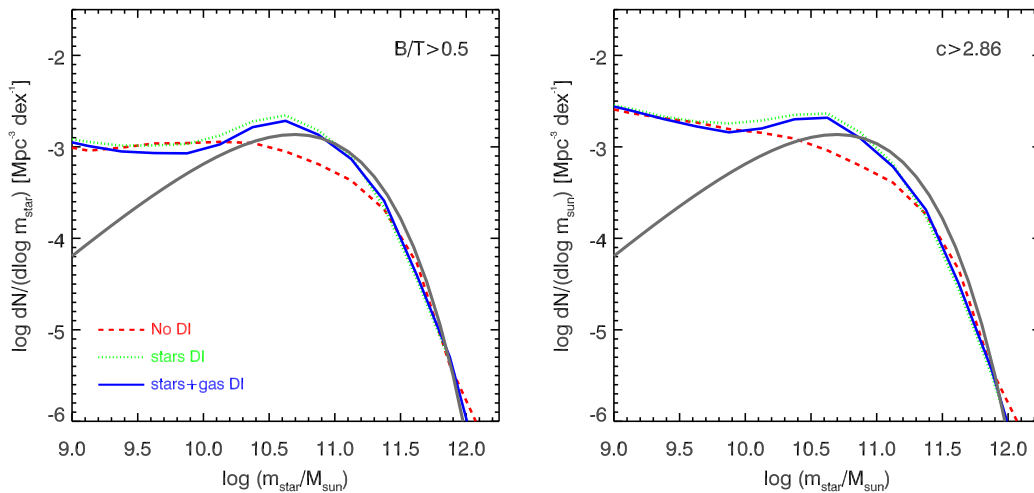


Figure 4. Stellar mass function for “early type” galaxies at redshift zero. In both panels, the gray curves show the observational estimate of the stellar mass function for galaxies with concentration $c > 2.86$ from Bernardi et al. (2010). The three colored lines show the ‘No DI’ (red), ‘Stars DI’ (green) and ‘Stars+Gas DI’ (blue) models. In the left panel, the models are selected according to the stellar mass bulge-to-total ratio ($B/T > 0.5$). In the right panel, we have assigned concentrations to the model galaxies using an empirical scaling (see text), and selected them to have $c > 2.86$. The model in which bulges form and grow only due to mergers (No DI) appears to underproduce early type galaxies in the mass range $\sim 2 \times 10^{10}$ to $\sim 3 \times 10^{11} M_{\odot}$.

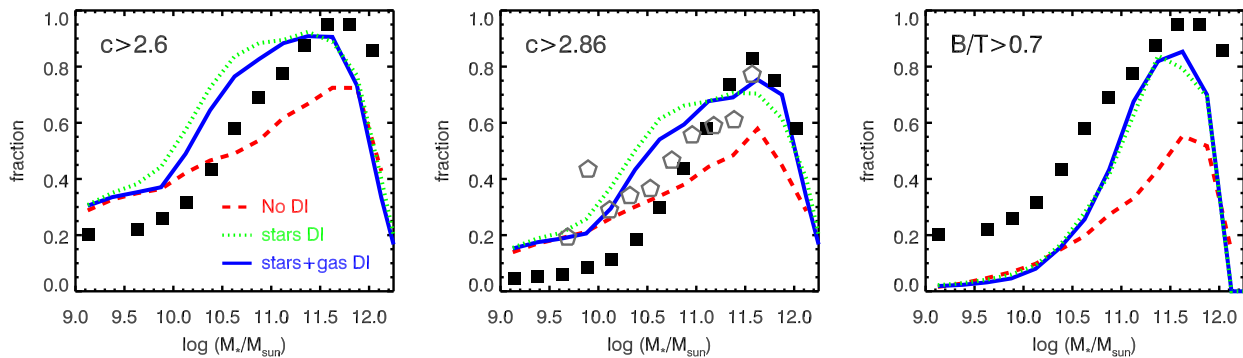


Figure 5. The fraction of “early type” galaxies at $z = 0$. The three colored lines show the ‘No DI’ (red), ‘Stars DI’ (green) and ‘Stars+Gas DI’ (blue) models. In the left panel, concentrations have been assigned to the model galaxies using an empirical scaling (see text), and the fraction of model galaxies with $c > 2.6$ is shown. The observed fraction of galaxies with $c > 2.6$ from Bernardi et al. (2010) is shown with the black square symbols. In the middle panel, model predictions and observational results are shown for galaxies with $c > 2.86$ in a similar manner. Observational estimates from the early-type sample classified by Cheng et al. (2011) are shown with open pentagons; this sample corresponds approximately to $B/T > 0.5$ or $c > 2.9$. In the right panel, we show model galaxies with stellar mass bulge-to-total ratio $B/T > 0.7$, compared with the early type sample of Hyde & Bernardi (2009), shown with filled squares. Again we see that the model without disk instabilities fails to produce enough spheroid-dominated galaxies at intermediate masses, regardless of the criteria used.

that mergers alone may not produce too many disks with large spheroids. However, our ‘stars’ and ‘stars+gas’ DI models do not produce enough disks with $B/T < 0.2$ and overproduce objects with intermediate B/T values.

Figure 7 shows the black hole-stellar bulge mass scaling relation for all galaxies at redshift zero. The three models produce nearly identical results, falling within the observational errors of McConnell & Ma (2013) at redshift zero — not surprising as the models have been tuned to match the normalization of the observed relationship. The models predict a shallower relation at low

bulge masses. This is due to the fact that galaxies are ‘seeded’ with a massive $10^5 M_{\odot}$ black hole, creating a floor in the black hole mass. We defer a comprehensive study of the evolution of the black hole scaling relations to future work (Hirschmann et al. in prep).

4.2 Growth of the stellar bulge

Figure 8 shows the evolution of the fraction of galaxies with different values of the bulge-to-total ratio as a function of stellar mass, from redshift zero to 1.75. We can

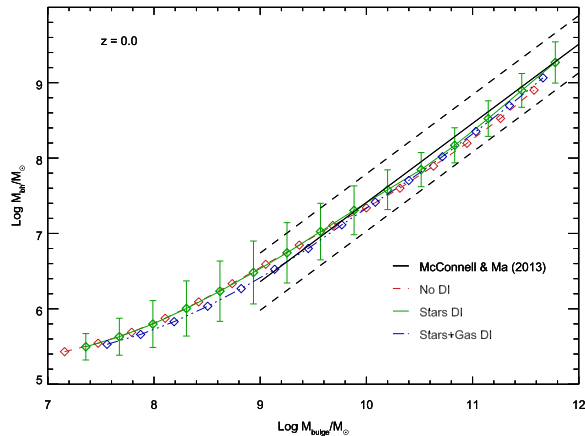


Figure 7. The black hole-stellar bulge scaling relation at $z = 0.0$ for the ‘No DI’ (red), ‘Stars DI’ (green) and ‘Stars+Gas DI’ (blue) models. The solid black line shows the $z = 0$ observed relation from McConnell & Ma (2013), with the dashed lines showing the $1 - \sigma$ scatter. The green error bars show the $1 - \sigma$ scatter for the ‘Stars DI’ model and are similar in magnitude to the scatter for the other two models. All three models have been tuned to reproduce the normalization of the observed $z = 0$ relation and show weak evolution with redshift. The relationship flattens at the low mass end due to the $10^5 M_\odot$ ‘seed’ black holes we have adopted in our models.

see that not only do the models with disk instabilities produce a larger fraction of spheroid-dominated galaxies, as we have already seen, but massive spheroids also form earlier in these models. In the models with spheroid growth via disk instabilities, massive galaxies become spheroid-dominated at high redshifts; above $10^{10.5} M_\odot$ the majority of galaxies are spheroid-dominated even at $z = 1.75$, while in the ‘No DI’ model, only about 30% of galaxies have $B/T > 0.5$. At low masses (lower than $10^{10} M_\odot$) there is no difference between the two models; disk instabilities evidently have little effect on low-mass disks in our SAMs.

4.3 Size-mass relation

In Figure 9, we show our model predictions for the size-mass relation of early-type galaxies at $z \sim 0$. We compare to a sample of SDSS galaxies (Hyde & Bernardi 2009; Shankar et al. 2010) that were selected to represent elliptical galaxies and minimize the contribution by disk galaxies; for this reason we limit the analysis to galaxies with stellar bulge-to-total ratios greater than 0.7. All three of our models that include dissipation predict a size-mass relationship that qualitatively agrees with the slope and dispersion of the observed relationship, falling within the $1 - \sigma$ error range for nearly three decades in stellar mass. We emphasize here that the model for bulge sizes is never explicitly tuned to observations; the only free parameters are constrained by hydrodynamical simulations. The fact that we predict a local size-mass relation that is in agreement with observations is thus a key finding of this paper.

For comparison, we also include a version of the model in which $C_{\text{rad}} = 0.0$ for all mergers. This dissipationless model produces galaxies that are too large

at all masses, with a size-mass relation that is nearly flat below $10^{10.5} M_\odot$. As described above, the amount of dissipation is tied to the amount of gas present in the merger. Since the gas fraction of disk-dominated galaxies increases with decreasing stellar mass (Kannappan 2004), low-mass spheroid-dominated galaxies are more likely to have formed via gas-rich processes. Furthermore, more massive spheroid-dominated galaxies are more likely to have undergone subsequent dry mergers, weakening the overall contribution from dissipation.

We now turn to the evolution of the size-mass relation to higher redshifts. Numerous observational studies (Trujillo et al. 2006; Marchesini et al. 2007; Toft et al. 2007; Williams et al. 2010) have shown that high-redshift quiescent galaxies are more compact than their low-redshift counterparts; here we compare to the results of a recent study by Newman et al. (2012).

Following Newman et al. (2012), we select all galaxies with specific star formation (sSFR) rates less than 0.02 Gyr^{-1} . For consistency with our other figures we also limit the population to spheroid-dominated galaxies ($B/T > 0.5$), although the results do not change if we include all quiescent galaxies. We have converted the Newman et al. (2012) results to a Chabrier IMF for consistency with our models. The median size-mass relation at redshifts 0, 0.75, 1.25, and 1.75 is shown in Figure 10.

All three models qualitatively reproduce the evolution of the mean size-mass relation since $z = 1.75$. We obtain similar results if we compare to Williams et al. (2010), using their evolving sSFR threshold (sSFR $< 0.3 t_H$, where t_H is the Hubble time at that redshift). We note that similar results are found above $10^{10.5} M_\odot$ if we use a mass-weighting instead of a luminosity-weighting, and if we use the bulge effective radius alone. Galaxies below $\sim 10^{10.5} M_\odot$ appear to have a shallower size-mass relationship above $z=1.25$. This is below the current limits of observational samples. The relation is steeper if we consider the size of the spheroid alone — evidently the flattening is due to the presence of a more extended disk in these low-mass systems.

4.4 Faber-Jackson relation and the Fundamental Plane

Observations have shown that early-type galaxies also fall on a tight relation between stellar mass and velocity dispersion, termed the Faber-Jackson (Faber & Jackson 1976, hereafter FJ) relation. While this relation is a power law to first order (Gallazzi et al. 2006), there are indications that it may be better approximated by a broken power law (Tortora et al. 2009) or a curve (Hyde & Bernardi 2009; Cappellari et al. 2012), in the sense that more massive galaxies have relatively lower velocity dispersions.

Our predicted FJ relation is shown in Figure 11. We find that the SAM reproduces the normalization of the relation at redshift zero (Gallazzi et al. 2006). While the high-redshift FJ relation is not yet well-constrained by observations, the SAM predicts that the normalization of the relation increases weakly with redshift, in agreement with observations (Cappellari et al. 2009).

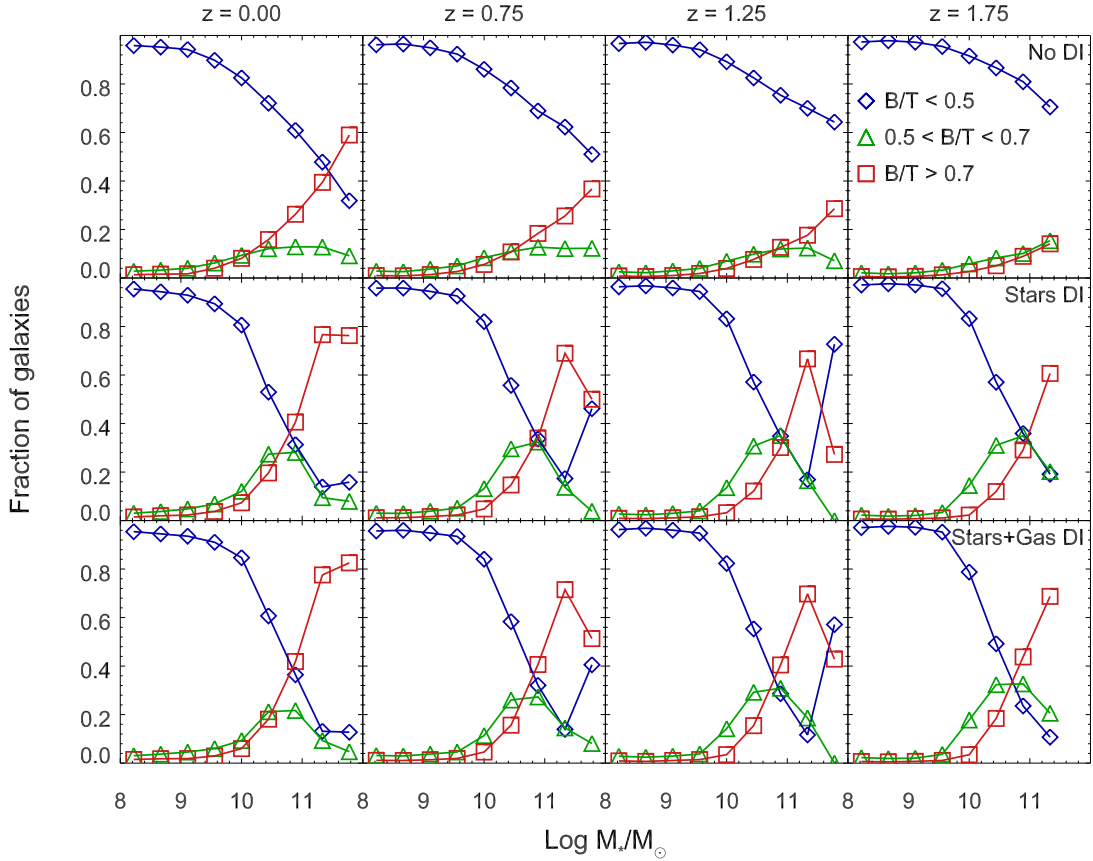


Figure 8. Fraction of galaxies with different bulge-to-total ratio as a function of stellar mass, at redshifts $z = 0.0, 0.75, 1.25,$ and 1.75 for the ‘No DI’ (top), ‘Stars DI’ (middle) and ‘Stars+Gas DI’ (bottom) versions of the SAM. The blue, green, and red lines indicate the fraction of galaxies of a given mass with stellar bulge-to-total ratios between $[0,0.5], [0.5,0.7],$ and $[0.7,1.0],$ respectively. All models predict a that a higher fraction of massive galaxies are spheroid-dominated; and spheroid-dominated galaxies form earlier in the models with disk instabilities.

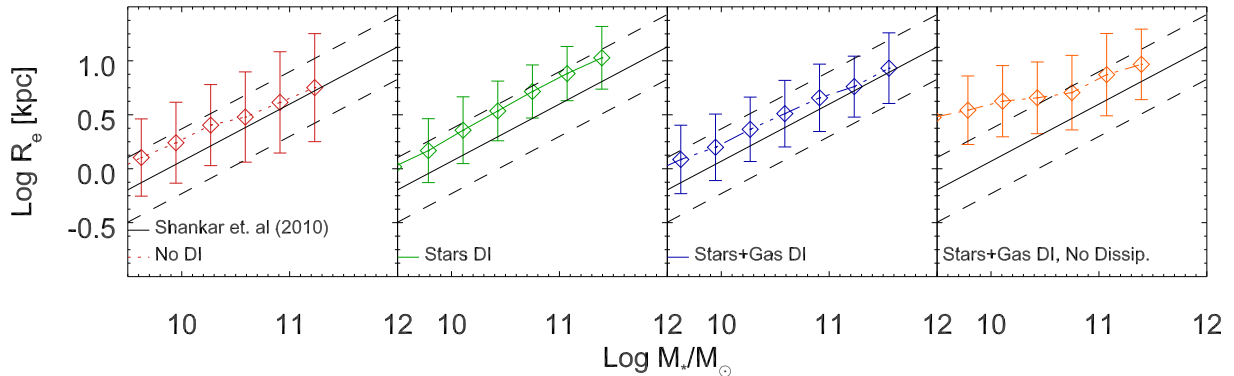


Figure 9. Size-mass relation for galaxies with $B/T > 0.7$ at redshift zero. The red, green, and blue lines show the ‘No DI’, ‘Stars DI’ and ‘Stars+Gas DI’ models with dissipation. The orange line shows the median relation for a model in which all mergers are considered to be dissipationless. The error bars represent the 1σ dispersion in the model predictions. The black line shows the observed local relation from Shankar et al. (2010). All dissipational models reproduce the slope of the observed scaling, while the dissipationless model produces a relation that is too flat, with low mass galaxies having sizes that are too large.

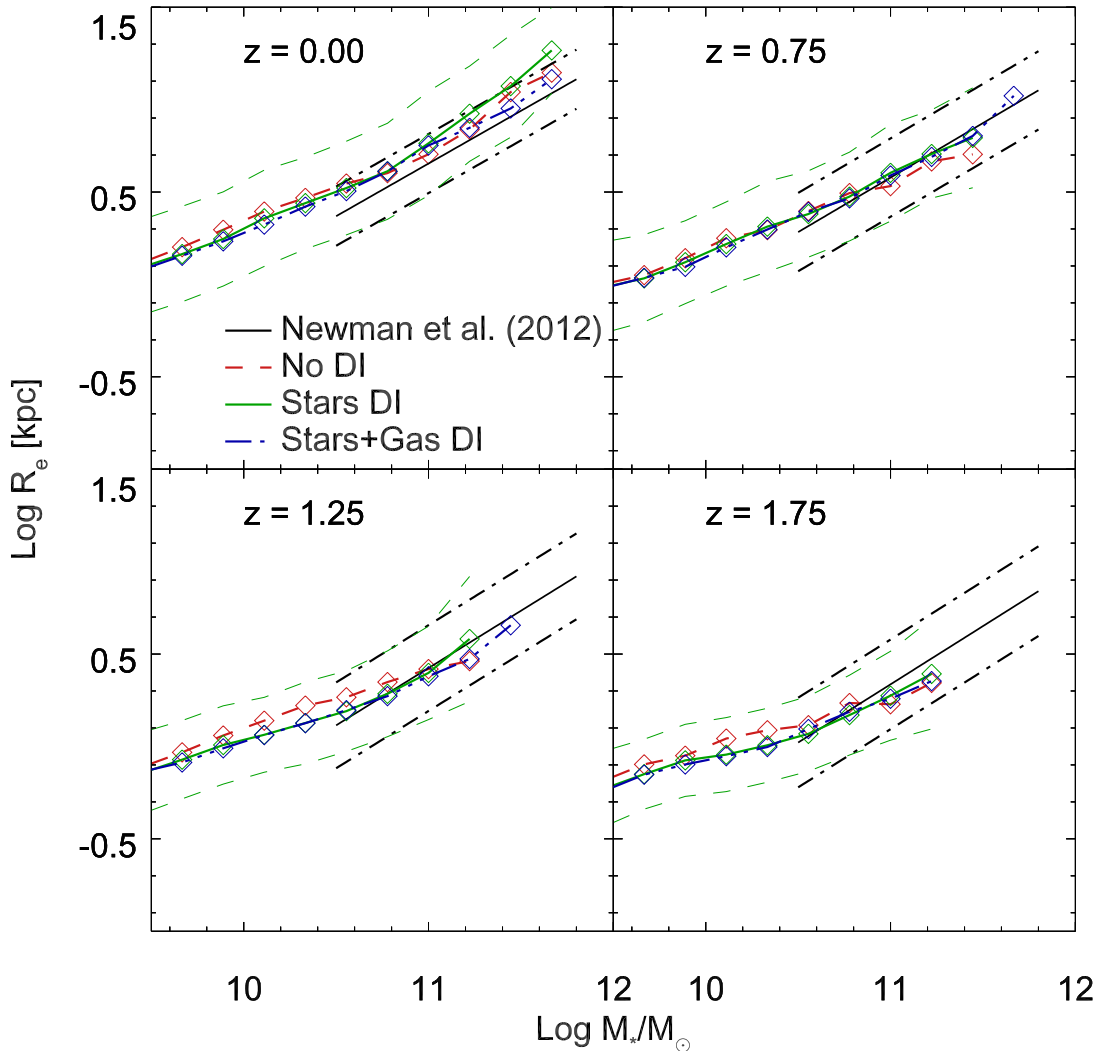


Figure 10. Size-mass relation for quiescent galaxies at redshift 0.0, 0.75, 1.25, and 1.75. The red, green, and blue lines show the ‘No DI’, ‘Stars DI’ and ‘Stars+Gas DI’ models with dissipation. The green dashed line shows the $1 - \sigma$ dispersion in the ‘Stars DI’ model; the other two models have similar dispersion. The black line shows the observed relation of Newman et al. (2012). All three models qualitatively reproduce the observed evolution.

The SAM agrees very well with the predictions of hydrodynamical simulations (Oser et al. 2012; Johansson et al. 2012) and observations of the evolution of the size-mass and Faber-Jackson relations at fixed stellar mass (Trujillo et al. 2006; Cappellari et al. 2009; Williams et al. 2010; Newman et al. 2012): galaxies at higher redshifts have higher velocity dispersions, but this evolution is much less dramatic than the evolution in the size-mass relation. Hydrodynamical simulations (Dekel & Cox 2006; Robertson et al. 2006a; Hopkins et al. 2010) have shown that galaxies that form via gas-rich processes will be compact, with high velocity dispersions. Simple analytic arguments (Naab et al. 2009) predict that dissipationless minor mergers can greatly increase the sizes of early-type galaxies while inducing only minor changes in the velocity dispersion.

In the SAM, this occurs because subsequent minor mergers increase the effective radius of the galaxy, enclosing more diffuse material within the effective radius.

Thus the evolution in the velocity dispersion indicates an evolution in the central surface density of galaxies. The fact that the SAM reproduces the *magnitude* of the evolution suggests that the overall SAM framework (i.e. the merger rate, gas fractions, etc.) can predict the evolution of galaxy properties to higher redshifts with reasonable accuracy.

While we reproduce the evolution in the normalization of the FJ relation, our models predict a curvature in the opposite direction to that seen in local observations. We predict velocity dispersions that are too high in the high-mass regime. This curvature seems to be a robust feature of our model, and we have checked that our results are not biased by a population of extremely compact galaxies, or galaxies too faint to be seen in the local universe.

One possibility is that the discrepancy at the high-mass end stems from variations in the stellar initial mass function (IMF). There is a growing body of ev-

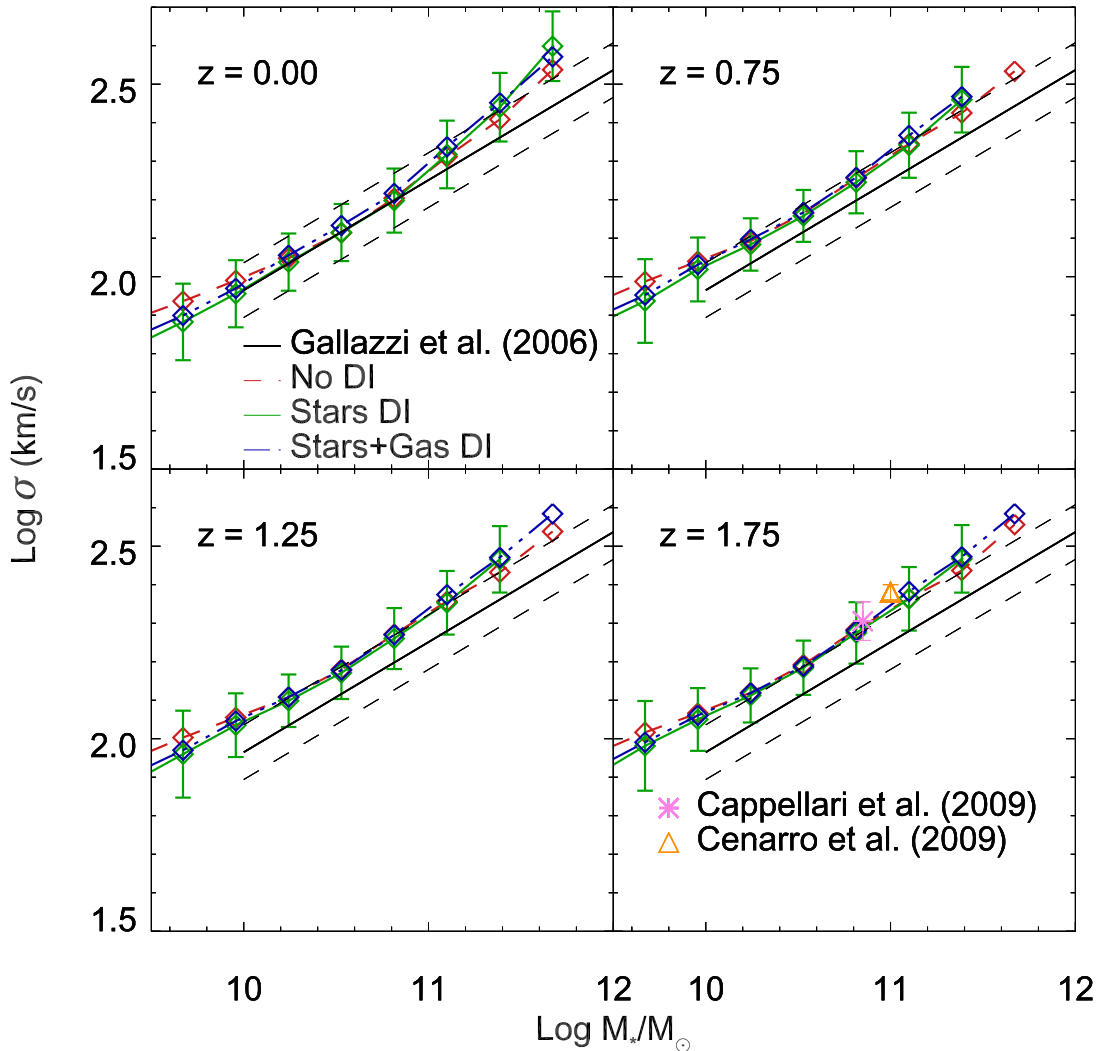


Figure 11. Faber-Jackson relation for spheroid-dominated galaxies at redshifts $z = 0.0, 0.75, 1.25,$ and 1.75 . The red, green, and blue lines show the ‘No DI’, ‘Stars DI’ and ‘Stars+Gas DI’ models. The green dashed line shows the $1 - \sigma$ dispersion in the ‘Stars DI’ model; the other two models have similar dispersion. The black line shows the observed $z = 0$ relation, with $1 - \sigma$ dispersion indicated by the dashed lines (Gallazzi et al. 2006). The pink star and orange triangle in the lower right panel show the average observed relations at $z \sim 1.6$ (Cappellari et al. 2009; Cenarro & Trujillo 2009). While the simulated galaxies match the zero-point of the observed low-redshift relation they display a curvature in the opposite direction from what is seen in observations. This discrepancy could perhaps be understood if the IMF varies with galaxy properties such as the velocity dispersion, as has been suggested by other studies (e.g. Conroy & van Dokkum 2012). The simulated galaxies agree with observations of the evolution in the normalization of the Faber-Jackson relation at higher redshifts.

idence (Cappellari et al. 2012; Conroy & van Dokkum 2012; Dutton et al. 2012) that early-type galaxies with high stellar masses or high velocity dispersions may have a bottom-heavy IMF (e.g. Salpeter), containing more low-mass stars relative to high-mass stars. Such an IMF would have a higher stellar mass-to-light ratio for a stellar population of a given age and metallicity.

Most observations, such as the Gallazzi et al. (2006) analysis, use stellar luminosities along with stellar population synthesis techniques to infer the stellar mass. Using an IMF that is too top-heavy for high-mass early-type galaxies would tend to underpredict the stellar masses of galaxies with high velocity dispersions: Conroy & van Dokkum (2012) estimate that stel-

lar mass-to-light ratios for a $\sigma > 300 \text{ km s}^{-1}$ galaxy may be twice that of the Milky Way. Such a correction would raise the high-mass end of the observed FJ relation by a factor of 0.3 dex. Of course, a non-universal IMF would also change the results of the SAM, though in a manner that is difficult to predict. For one thing, the parameters of the SAM would have to be re-adjusted to fit the revised estimates of the stellar mass function.

We now turn to the Fundamental Plane, which we consider in the projection $M_{\text{star}} \propto (\sigma^2 R_e)^\alpha$. If all galaxies had the same mass-to-light ratio then one would expect a simple virial scaling, with $\alpha = 2$. However observations (Faber et al. 1987; Djorgovski & Davis 1987; Dressler et al. 1987) have shown that the true FP is

tilted from the virial relation, with estimates of the scaling near $\alpha \sim 1.2$ (Pahre et al. 1998; Padmanabhan et al. 2004; Gallazzi et al. 2006). Hydrodynamical simulations (Dekel & Cox 2006; Robertson et al. 2006b; Covington et al. 2008) have shown that if low-mass galaxies have higher gas fractions, they will experience more dissipation in mergers. These galaxies will have higher concentrations of baryonic matter and lower dark matter fractions within their effective radii, producing a tilt in the Fundamental Plane. Here we examine this tilt in a cosmological context.

As there is some evidence that galaxies with large pseudobulges may have a different FP tilt (Kormendy & Fisher 2008) and the observations we are comparing to either limit their samples to galaxies with high Sérsic indices or fit galaxies to a de Vaucouleurs $n = 4$ profile, we restrict this analysis to galaxies that have grown at least half of their bulge mass through mergers; in practice this restriction has a minimal effect on the results. For our chosen set of FP variables there is no dependence on the stellar mass-to-light ratio; any tilt in the FP comes from variations in the internal structure of the galaxies. We find that the SAM closely reproduces the observed local scaling of $\alpha \approx 1.2$ and, in agreement with observations, the scatter in the FP is smaller than the scatter in either the size-mass or Faber-Jackson relations. We find a slight steepening in the FP at high masses ($M_* > 10^{11.5} M_\odot$), which is generally consistent with high-redshift observations showing minimal evolution or a slight increase in the stellar-to-dynamical mass ratio with redshift (Holden et al. 2010; Toft et al. 2012; Bezanson et al. 2013). There is no dependence on stellar bulge-to-total ratio, and the differences between the results of the three model variants (‘No DI’, ‘stars DI’, ‘stars+gas’ DI) are small.

We find only a minor decrease in the normalization of the FP and a slightly stronger decrease in the tilt of the FP with redshift. Performing a least-squares linear fit to the FP relation, we find a coefficient of $\alpha = 1.21$ at redshift zero, consistent with observations, evolving to $\alpha = 1.11$ at $z = 1.75$. The evolution of this tilt supports a scenario in which mergers at lower redshifts involve less dissipation due to the lower gas content of the progenitors. While subsequent dry mergers are thought to preserve the tilt (Robertson et al. 2006b) induced by the formative event, the population is continuously supplanted with the products of increasingly gas-poor mergers. In this way the tilt of the FP may slowly evolve over time.

5 DISCUSSION AND CONCLUSIONS

We have updated the “Santa Cruz” (Somerville et al. 2008a, 2012) semi-analytic model to run within accurate merger trees extracted from the Bolshoi N-body simulation, and to predict the structural properties of spheroids, using an analytic model (Covington et al. 2008; Covington et al. 2011) based on hydrodynamical simulations of binary galaxy mergers (Johansson et al. 2009). These simulations allow us to parameterize the amount of dissipation that occurs during a merger based on the mass ratio, gas content, size, morphology, and or-

bit of the progenitor galaxies. The hydrodynamical simulations also show that the velocity dispersion can be determined simply by using the virial theorem, accounting for the amount of dark matter in the center of the galaxy.

In agreement with some previous studies, we find that a model in which spheroids grow only via mergers has difficulty reproducing the observed number density of intermediate-mass spheroid-dominated galaxies at $z = 0$. We therefore investigate two different prescriptions for spheroid growth via disk instabilities, one in which only stars determine and participate in the disk instability, and one in which both stars and gas are involved. Massive spheroids form considerably earlier in both of these models compared with the ‘No DI’ model, and this may provide a future observational test of the physical mechanisms included in the models.

All three model variants qualitatively reproduce the slope, zero-point, scatter and evolution of the size-mass relation for early-type galaxies. The models with disk instabilities produce better agreement with these observations than the ‘No DI’ model. We emphasize that the model has not been tuned to reproduce these observations; the free parameters in our merger model were instead chosen based on the results of hydrodynamical binary merger simulations. We have shown that the success of this model is due to our treatment of dissipation in gas-rich mergers; if we neglect dissipation the model predicts a much flatter size-mass relation, in conflict with observations. Similar results can be seen in other SAMs that model spheroid sizes without versus with the inclusion of dissipation (Guo et al. 2011; Shankar et al. 2013).

Covington et al. (2011) presented predictions based on a similar model, applied to merger progenitors selected from the Santa Cruz and Millennium (Croton et al. 2006) SAMs in post-processing. They argued that the “steepening” of the size-mass relation for early types relative to late types, as well as its smaller scatter and more rapid evolution, could be qualitatively understood with reference to the role of dissipation in mergers, as described in their study. If there is a negative correlation between galaxy gas fraction and stellar mass, such that lower mass galaxies have higher cold gas fractions (as observed), then mergers between lower mass galaxies experience more dissipation and result in more compact remnants. This will therefore result in a size-mass relation for the remnants that is steeper than the progenitor size-mass relation. Second, they showed that disk galaxies with larger radius at a given stellar mass have higher gas fractions, due to the gas surface density dependent star formation efficiency implemented via the usual Kennicutt-Schmidt relation. Therefore, larger disks also experience more dissipation, leading to a *tightening* in the size-mass relation for the remnants relative to the progenitors. Third, if galaxy cold gas fractions were higher at high redshift, early types formed at lower redshift will experience less dissipation, and therefore form more extended remnants, leading to evolution in the size-mass relation that is more rapid than that in the progenitor population. They also showed that the observed “tilt” in the Fundamental Plane can be reproduced in their models; the change in tilt relative to the virial relation is due to the changing central

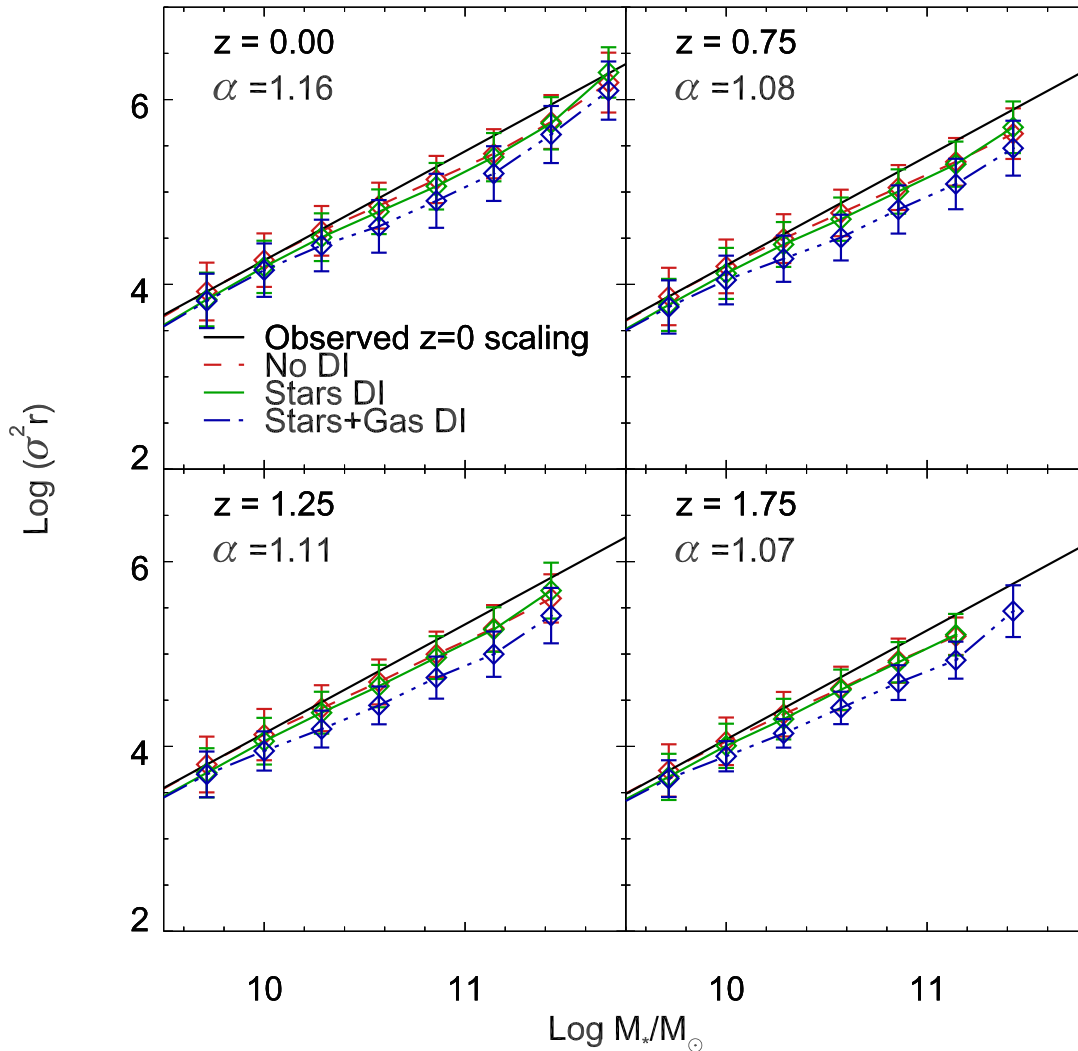


Figure 12. Projected Fundamental Plane at redshifts $z = 0.0, 0.75, 1.25,$ and 1.75 . The red, green, and blue lines show the ‘No DI’, ‘Stars DI’ and ‘Stars+Gas DI’ models. Only spheroid-dominated galaxies that grew bulges mainly through mergers are shown here. Error bars show the $1\text{-}\sigma$ dispersion in the model predictions. The slope of the FP in the ‘Stars DI’ model at each redshift is denoted by α . In the local universe the SAM reproduces the observed tilt of the FP, $\alpha \approx 1.2$, and shows only minor evolution towards higher redshift. Any evolution in the zero-point with redshift is within the $1\text{-}\sigma$ errors.

dark matter fraction that again results from the mass dependence of progenitor gas fraction. These are all important insights into the possible mechanisms that drive the origin and evolution of galaxy structural scaling relations.

However, the Covington et al. study had several important limitations. It was based on simulations that only considered mergers between relatively gas rich, disk-dominated progenitors. Moreover, the calculations were applied in post-processing on SAM disk-dominated galaxies that had experienced a recent major merger. Thus all early type galaxies that formed through mergers at much earlier times were not included in the populations that were examined. In addition, the effects of minor mergers, multiple mergers, and mixed-morphology mergers were neglected. As a result, the Covington approach was not able to reproduce, for example, the observed stellar mass functions of disk and spheroid dominated galaxies

at the present day. In this work, we extend the Covington model by calibrating a wider variety of mergers using a new analysis of the Johansson et al. (2009) merger simulations. We then implement the model *self-consistently* within the Santa Cruz SAM.

The results of our more detailed and realistic model provide even stronger support in favor of all of the dissipation-related insights presented in Covington, summarized above. To these, we add the important new insight that *major and minor mixed-morphology mergers (D-B and B-d) behave like dissipationless mergers*. These mixed-morphology mergers become increasingly common at redshifts less than about $z \sim 1.2$, and may play a significant role in the build-up of the extended envelopes observed in giant elliptical galaxies in the local universe. The significantly better quantitative agreement with the evolution of the observed size-mass relation for early type galaxies that we now obtain with our more sophisticated

model also implies that *several other effects* beyond the ones already discussed in Covington et al. also contribute to the observed size evolution, as discussed below.

It has been suggested that the strong evolution in the size-mass relation for spheroid-dominated galaxies may be driven largely by minor mergers (e.g. Naab et al. 2007; Naab et al. 2009). However, some recent studies have suggested that the minor merger rate may not be sufficient to account for the observed evolution in the size-mass relation, particularly above $z \sim 1$ (Newman et al. 2012; Shankar et al. 2013). Our results suggest that several other effects may contribute to the size evolution as well. The papers previously mentioned treat only gas-poor mergers as dissipationless. However, the hydrodynamical simulations we have analyzed show that mergers between a disk-dominated and a spheroid-dominated galaxy behave as though they were dissipationless as well. Since spiral galaxies tend to be larger than elliptical galaxies at a given mass at all redshifts, these mergers will greatly increase the effective radii of early-type galaxies, even more than mergers between two dry spheroids. In addition, in our models, high-redshift spheroid-dominated galaxies can regrow a disk; this process removes some compact early-type galaxies from the population at lower redshifts. The evolution of the gas fraction with redshift also means that the role of dissipation changes over time, with early, “wet” mergers producing more compact remnants, and later, “dry” mergers producing more diffuse spheroids. In a forthcoming paper (Somerville, Porter et al. in prep), we investigate and elucidate the physical processes responsible for spheroid growth in our models in more detail.

Our models predict a slight curvature in the Faber-Jackson relation at high stellar masses that is not seen in observations, but at lower stellar masses, the model reproduces the slope and normalization of the relation. At higher redshifts we predict a mild increase in velocity dispersion at fixed mass, in agreement with recent observations. Our models also match the tilt of the projected Fundamental Plane ($M_* \propto \sigma^2 r$) at redshift zero. We predict a slight decrease in this tilt to higher redshifts; however the magnitude of this change is well within the measurement errors of high-redshift observations.

Although we consider the results presented here to be promising, our existing models have a number of limitations and remaining uncertainties. Our treatment of disk instabilities is one of the most uncertain aspects of our models. Both SAMs and hydrodynamical simulations point to the importance of disk instabilities in forming spheroids (Dekel et al. 2009a; De Lucia et al. 2011; Genel et al. 2012a), but the details of the criteria that determine when a disk becomes unstable, and what happens to it when it does, remain highly uncertain. Furthermore, our models do not include any environmental effects such as ram pressure or tidal stripping or harassment, which may also contribute to galaxy morphological transformation. In addition, the hydrodynamic simulations upon which we based our recipes for spheroid formation in mergers are binary mergers of idealized galaxies that are not in a proper cosmological context. In particular, they do not have hot gas halos or cosmological accretion. Nor do they account for “multiple mergers” (merg-

ers which occur before a galaxy has come to equilibrium following a previous merger), which may have different dynamical effects and are predicted to be common in a Λ CDM universe (Moster et al. 2014). The coming generation of high-resolution hydrodynamic “zoom-in” simulations, including realistic recipes for stellar feedback, black hole growth, and AGN feedback, confronted with the results from high-resolution deep imaging surveys, will shed more light on the physical processes that shape the structure and evolution of galactic spheroids.

6 ACKNOWLEDGMENTS

We thank Avishai Dekel, Sandra Faber, Susan Kassin, David Koo, Yu Lu, Thorsten Naab, and Jerry Sellwood for interesting and useful conversations. LP and JP acknowledge funding from NSF-AST 1010033 and HST-GO-12060.12-A (CANDELS). PHJ acknowledges the support of the Research Funds of the University of Helsinki and the Magnus Ehrnrooth Foundation.

REFERENCES

- Athanassoula E., 2008, MNRAS, 390, L69
 Auger M. W., Treu T., Gavazzi R., Bolton A. S., Koopmans L. V. E., Marshall P. J., 2010, ApJ, 721, L163
 Baldry I. K., Glazebrook K., Brinkmann J., Ivezić Ž., Lupton R. H., Nichol R. C., Szalay A. S., 2004, ApJ, 600, 681
 Barnes J. E., Hernquist L., 1996, AJ, 471, 115
 Barro G. et al., 2013, ApJ, 765, 104
 Behroozi P. S., Wechsler R. H., Wu H.-Y., Busha M. T., Klypin A. A., Primack J. R., 2013, ApJ, 763, 18
 Bell E. F., Zheng X. Z., Papovich C., Borch A., Wolf C., Meisenheimer K., 2007, ApJ, 663, 834
 Benson A. J., Bower R., 2010, MNRAS, 405, 1573
 Benson A. J., Devereux N., 2010, MNRAS, 402, 2321
 Bernardi M., Meert A., Sheth R. K., Vikram V., Huertas-Company M., Mei S., Shankar F., 2013, MNRAS, 436, 697
 Bernardi M., Shankar F., Hyde J. B., Mei S., Marulli F., Sheth R. K., 2010, MNRAS, 404, 2087
 Bezanson R., van Dokkum P., van de Sande J., Franx M., Kriek M., 2013, ApJL, 764, L8
 Bezanson R. et al., 2011, ApJL, 737, L31
 Birnboim Y., Dekel A., 2003, MNRAS, 345, 349
 Blanton M. R., Moustakas J., 2009, ARA&A, 47, 159
 Bondi H., 1952, MNRAS, 112, 195
 Bournaud F. et al., 2011, ApJ, 730, 4
 Bower R. G., Benson A. J., Malbon R., Helly J. C., Frenk C. S., Baugh C. M., Cole S., Lacey C. G., 2006, MNRAS, 370, 645
 Boylan-Kolchin M., Ma C.-P., Quataert E., 2008, MNRAS, 383, 93
 Brammer G. B. et al., 2011, ApJ, 739, 24
 Bruzual G., Charlot S., 2003, MNRAS, 344, 1000
 Buitrago F., Trujillo I., Conselice C. J., Bouwens R. J., Dickinson M., Yan H., 2008, ApJ, 687, L61
 Bundy K. et al., 2008, ApJ, 681, 931

- Burstein D., Bender R., Faber S., Nolthenius R., 1997, *AJ*, 114, 1365
- Cappellari M. et al., 2009, *ApJL*, 704, L34
- Cappellari M. et al., 2012, *Nat*, 484, 485
- Cassata P. et al., 2013, *ApJ*, 775, 106
- Cenarro A. J., Trujillo I., 2009, *ApJL*, 696, L43
- Ceverino D., Dekel A., Bournaud F., 2010, *MNRAS*, 404, 2151
- Chabrier G., 2003, *PASP*, 115, 763
- Cheng J. Y., Faber S. M., Simard L., Graves G. J., Lopez E. D., Yan R., Cooper M. C., 2011, *MNRAS*, 412, 727
- Christodoulou D. M., Shlosman I., Tohline J. E., 1995, *ApJ*, 443, 551
- Cole S., Aragon-Salamanca A., Frenk C. S., Navarro J. F., Zepf S. E., 1994, *MNRAS*, 271, 781
- Cole S., Lacey C. G., Baugh C. M., Frenk C. S., 2000, *MNRAS*, 319, 168
- Combes F., Debbasch F., Friedli D., Pfenniger D., 1990, *A&A*, 233, 82
- Conroy C., van Dokkum P. G., 2012, *ApJ*, 760, 71
- Cook M., Barausse E., Evoli C., Lapi A., Granato G. L., 2010, *MNRAS*, 402, 2113
- Covington M., Dekel A., Cox T. J., Jonsson P., Primack J. R., 2008, *MNRAS*, 384, 94
- Covington M. D., Primack J. R., Porter L. A., Croton D. J., Somerville R. S., Dekel A., 2011, *MNRAS*, 1029
- Cox T. J., 2004, PhD thesis, UC Santa Cruz
- Cox T. J., Dutta S. N., Di Matteo T., Hernquist L., Hopkins P. F., Robertson B., Springel V., 2006, *ApJ*, 650, 791
- Cox T. J., Dutta S. N., Matteo T. D., Hernquist L., Hopkins P. F., Robertson B., Springel V., 2006, *ApJ*, 650, 791
- Cox T. J., Jonsson P., Primack J. R., Somerville R. S., 2006, *MNRAS*, 373, 1013
- Cox T. J., Jonsson P., Somerville R. S., Primack J. R., Dekel A., 2008, *MNRAS*, 384, 386
- Croton D. J. et al., 2006, *MNRAS*, 365, 11
- Daddi E. et al., 2005, *ApJ*, 626, 680
- De Lucia G., Fontanot F., Wilman D., Monaco P., 2011, *MNRAS*, 517
- De Lucia G., Springel V., White S. D. M., Croton D., Kauffmann G., 2006, *MNRAS*, 366, 499
- Debattista V. P., Carollo C. M., Mayer L., Moore B., 2004, *ApJL*, 604, L93
- Dekel A. et al., 2009a, *Nat*, 457, 451
- Dekel A., Cox T. J., 2006, *MNRAS*, 370, 1445
- Dekel A., Sari R., Ceverino D., 2009b, *ApJ*, 703, 785
- Di Matteo T., Springel V., Hernquist L., 2005, *Nature*, 433, 604
- Djorgovski S., Davis M., 1987, *ApJ*, 313, 59
- Dressler A., Lynden-Bell D., Burstein D., Davies R. L., Faber S. M., Terlevich R., Wegner G., 1987, *ApJ*, 313, 42
- Dutton A. A., Mendel J. T., Simard L., 2012, *MNRAS*, 422, L33
- Efstathiou G., Lake G., Negroponte J., 1982, *MNRAS*, 199, 1069
- Elmegreen B. G., Bournaud F., Elmegreen D. M., 2008, *ApJ*, 688, 67
- Elmegreen D. M., Elmegreen B. G., Marcus M. T., Shahinyan K., Yau A., Petersen M., 2009, *ApJ*, 701, 306
- Faber S. M., Dressler A., Davies R. L., Burstein D., Lynden-Bell D., 1987, in *Nearly Normal Galaxies. From the Planck Time to the Present*, ed. S. M. Faber (New York, NY: Springer-Verlag), 175
- Faber S. M., Jackson R. E., 1976, *ApJ*, 204, 668
- Faber S. M., et al., 2007, *ApJ*, 665, 265
- Fabian A. C., 2012, *ARA&A*, 50, 455
- Fall S. M., Efstathiou G., 1980, *MNRAS*, 193, 189
- Font A. S. et al., 2008, *MNRAS*, 389, 1619
- Fontanot F., Cristiani S., Santini P., Fontana A., Grazian A., Somerville R. S., 2012, *MNRAS*, 421, 241
- Fontanot F., De Lucia G., Monaco P., Somerville R. S., Santini P., 2009, *MNRAS*, 397, 1776
- Forbes D. A., Spitler L. R., Strader J., Romanowsky A. J., Brodie J. P., Foster C., 2011, *MNRAS*, 413, 2943
- Gadotti D. A., 2009, *MNRAS*, 393, 1531
- Gallazzi A., Charlot S., Brinchmann J., White S. D. M., 2006, *MNRAS*, 370, 1106
- Genel S., Dekel A., Cacciato M., 2012a, *MNRAS*, 3466
- Genel S. et al., 2012b, *ApJ*, 745, 11
- Genzel R. et al., 2011, *ApJ*, 733, 101
- Gnedin N. Y., 2000, *ApJ*, 542, 535
- Gnedin O. Y., 2003, *ApJ*, 582, 141
- González J. E., Lacey C. G., Baugh C. M., Frenk C. S., Benson A. J., 2009, *MNRAS*, 397, 1254
- Gunn J. E., Gott J. R. I., 1972, *ApJ*, 176, 1
- Guo Q. et al., 2011, *MNRAS*, 413, 101
- Guo Y., Giavalisco M., Ferguson H. C., Cassata P., Koekemoer A. M., 2012, *ApJ*, 757, 120
- Hatton S., Devriendt J. E. G., Ninin S., Bouchet F. R., Guiderdoni B., Vibert D., 2003, *MNRAS*, 343, 75
- Hirschmann M., Somerville R. S., Naab T., Burkert A., 2012, *MNRAS*, 426, 237
- Hohl F., 1971, *ApJ*, 168, 343
- Holden B. P., van der Wel A., Kelson D. D., Franx M., Illingworth G. D., 2010, *ApJ*, 724, 714
- Hopkins A. M., Beacom J. F., 2008, *ApJ*, 682, 1486
- Hopkins P. F., Bundy K., Hernquist L., Wuyts S., Cox T. J., 2010, *MNRAS*, 401, 1099
- Hopkins P. F., Bundy K., Murray N., Quataert E., Lauer T. R., Ma C.-P., 2009, *MNRAS*, 398, 898
- Hopkins P. F., Cox T. J., Kereš D., Hernquist L., 2008, *ApJS*, 175, 390
- Hopkins P. F., Cox T. J., Younger J. D., Hernquist L., 2009a, *ApJ*, 691, 1168
- Hopkins P. F., Hernquist L., Cox T. J., Keres D., Wuyts S., 2009b, *ApJ*, 691, 1424
- Hopkins P. F., Hernquist L., Cox T. J., Robertson B., Di Matteo T., Springel V., 2006, *ApJ*, 639, 700
- Hopkins P. F., Hernquist L., Cox T. J., Robertson B., Krause E., 2007, *ApJ*, 669, 45
- Hopkins P. F., Lauer T. R., Cox T. J., Hernquist L., Kormendy J., 2009c, *ApJS*, 181, 486
- Hopkins P. F. et al., 2009d, *MNRAS*, 397, 802
- Hyde J. B., Bernardi M., 2009, *MNRAS*, 394, 1978
- Johansson P. H., Naab T., Burkert A., 2009, *ApJ*, 690, 802
- Johansson P. H., Naab T., Ostriker J. P., 2012, *ApJ*, 754, 115

- Jørgensen I., Franx M., Kjaergaard P., 1996, *MNRAS*, 280, 167
- Kannappan S. J., 2004, *ApJ*, 611, L89
- Kauffmann G., White S. D. M., 1993, *MNRAS*, 261, 921
- Kennicutt R. C., 1998, *ApJ*, 498, 541
- Kennicutt, Jr. R. C., 1988, *ApJ*, 334, 144
- Kereš D., Katz N., Weinberg D. H., Davé R., 2005, *MNRAS*, 363, 2
- Khochfar S., Burkert A., 2003, *ApJL*, 597, L117
- Khochfar S., Silk J., 2006, *ApJL*, 648, L21
- Kimm T. et al., 2009, *MNRAS*, 394, 1131
- Klypin A. A., Trujillo-Gomez S., Primack J., 2011, *ApJ*, 740, 102
- Komatsu E. et al., 2009, *ApJS*, 180, 330
- Komatsu E. et al., 2011, *ApJS*, 192, 18
- Kormendy J., Fisher D. B., 2008, in *Formation and Evolution of Galaxy Disks ASP Conference Series*, p. 297
- Koushiappas S. M., Bullock J. S., Dekel A., 2004, *MNRAS*, 354, 292
- Kravtsov A. V., Gnedin O. Y., Klypin A. A., 2004, *ApJ*, 609, 482
- Leroy A. K., Walter F., Brinks E., Bigiel F., de Blok W. J. G., Madore B., Thornley M. D., 2008, *AJ*, 136, 2782
- Li C., White S. D. M., 2009, *MNRAS*, 398, 2177
- Loeb A., Rasio F. A., 1994, *ApJ*, 432, 52
- Lotz J. M., Jonsson P., Cox T. J., Croton D., Primack J. R., Somerville R. S., Stewart K., 2011, *ApJ*, 742, 103
- Lu Y. et al., 2013, *ArXiv e-prints*, 1312.3233
- Marchesini D. et al., 2007, *ApJ*, 656, 42
- McConnell N. J., Ma C.-P., 2013, *ApJ*, 764, 184
- Mihos J. C., Hernquist L., 1994a, *ApJ*, 437, L47
- Mihos J. C., Hernquist L., 1994b, *ApJ*, 431, L9
- Mo H. J., Mao S., White S. D. M., 1998, *MNRAS*, 295, 319
- Moore B., Katz N., Lake G., Dressler A., Oemler A., 1996, *Nat*, 379, 613
- Moore B., Lake G., Katz N., 1998, *ApJ*, 495, 139
- Moster B. P., Macciò A. V., Somerville R. S., 2014, *MNRAS*, 437, 1027
- Moustakas J. et al., 2013, *ApJ*, 767, 50
- Muzzin A. et al., 2013, *ApJ*, 777, 18
- Naab T., Jesseit R., Burkert A., 2006, *MNRAS*, 372, 839
- Naab T., Johansson P. H., Ostriker J. P., 2009, *ApJL*, 699, L178
- Naab T., Johansson P. H., Ostriker J. P., Efstathiou G., 2007, *ApJ*, 658, 710
- Navarro J. F., Frenk C. S., White S. D. M., 1997, *ApJ*, 490, 493
- Newman A. B., Ellis R. S., Bundy K., Treu T., 2012, *ApJ*, 746, 162
- Oser L., Naab T., Ostriker J. P., Johansson P. H., 2012, *ApJ*, 744, 63
- Oser L., Ostriker J. P., Naab T., Johansson P. H., Burkert A., 2010, *ApJ*, 725, 2312
- Ostriker J. P., Peebles P. J. E., 1973, *ApJ*, 186, 467
- Padmanabhan N. et al., 2004, *New Astronomy*, 9, 329
- Pahre M. A., Djorgovski S. G., de Carvalho R. R., 1998, *ApJ*, 116, 1591
- Panter B., Jimenez R., Heavens A. F., Charlot S., 2007, *MNRAS*, 378, 1550
- Parry O. H., Eke V. R., Frenk C. S., 2009, *MNRAS*, 396, 1972
- Parry O. H., Eke V. R., Frenk C. S., 2009, *MNRAS*, 396, 1972
- Prugniel P., Simien F., 1997, *A&A*, 321, 111
- Robaina A. R., Bell E. F., van der Wel A., Somerville R. S., Skelton R. E., McIntosh D. H., Meisenheimer K., Wolf C., 2010, *ApJ*, 719, 844
- Robertson B., Bullock J. S., Cox T. J., Matteo T. D., Hernquist L., Springel V., Yoshida N., 2006a, *ApJ*, 645, 986
- Robertson B., Cox T. J., Hernquist L., Franx M., Hopkins P. F., Martini P., Springel V., 2006b, *ApJ*, 641, 21
- Shankar F., Marulli F., Bernardi M., Boylan-Kolchin M., Dai X., Khochfar S., 2010, *MNRAS*, 405, 948
- Shankar F., Marulli F., Bernardi M., Dai X., Hyde J. B., Sheth R. K., 2010, *MNRAS*, 403, 117
- Shankar F., Marulli F., Bernardi M., Mei S., Meert A., Vikram V., 2013, *MNRAS*, 428, 109
- Shen S., Mo H. J., White S. D. M., Blanton M. R., Kauffmann G., Voges W., Brinkmann J., Csabai I., 2003, *MNRAS*, 343, 978
- Somerville R. S. et al., 2008a, *ApJ*, 672, 776
- Somerville R. S., Gilmore R. C., Primack J. R., Domínguez A., 2012, *MNRAS*, 2820
- Somerville R. S., Hopkins P. F., Cox T. J., Robertson B. E., Hernquist L., 2008b, *MNRAS*, 391, 481
- Somerville R. S., Primack J. R., 1999, *MNRAS*, 310, 1087
- Somerville R. S., Primack J. R., Faber S. M., 2001, *MNRAS*, 320, 504
- Springel V., 2005, *MNRAS*, 364, 1105
- Springel V., Di Matteo T., Hernquist L., 2005, *ApJ*, 620, L79
- Springel V., Di Matteo T., Hernquist L., 2005, *MNRAS*, 361, 776
- Springel V., Hernquist L., 2003, *MNRAS*, 339, 289
- Sutherland R. S., Dopita M. A., 1993, *ApJS*, 88, 253
- Syer D., Mao S., Mo H. J., 1999, *MNRAS*, 305, 357
- Szomoru D., Franx M., van Dokkum P. G., 2012, *ApJ*, 749, 121
- Toft S., Gallazzi A., Zirm A., Wold M., Zibetti S., Grillo C., Man A., 2012, *ApJ*, 754, 3
- Toft S. et al., 2007, *ApJ*, 671, 285
- Toomre A., 1964, *ApJ*, 139, 1217
- Tortora C., Napolitano N. R., Romanowsky A. J., Cappacioli M., Covone G., 2009, *MNRAS*, 396, 1132
- Trujillo I., Conselice C. J., Bundy K., Cooper M. C., Eisenhardt P., Ellis R. S., 2007, *MNRAS*, 382, 109
- Trujillo I. et al., 2006, *ApJ*, 650, 18
- Trujillo-Gomez S., Klypin A., Primack J., Romanowsky A. J., 2011, *ApJL*, 742, 16
- van Dokkum P. G. et al., 2008, *ApJL*, 677, L5
- van Dokkum P. G. et al., 2010, *ApJ*, 709, 1018
- Volonteri M., Stark D. P., 2011, *MNRAS*, 417, 2085
- Weinzirl T., Jogee S., Khochfar S., Burkert A., Kormendy J., 2009, *ApJ*, 696, 411
- Wetzell A. R., 2010, *ApJ*, 412, 49
- Whitaker K. E., van Dokkum P. G., Brammer G., Franx M., 2012, *ApJL*, 754, L29
- White S. D. M., Frenk C. S., 1991, *ApJ*, 379, 52

Williams R. J., Quadri R. F., Franx M., van Dokkum
P., Toft S., Kriek M., Labbé I., 2010, *ApJ*, 713, 738
Wilman D. J., Fontanot F., De Lucia G., Erwin P.,
Monaco P., 2013, *MNRAS*, 433, 2986
Wuyts S. et al., 2012, *ApJ*, 753, 114
Wuyts S. et al., 2011, *ApJ*, 742, 96